Supporting Information for

Single-atomic cobalt sites embedded in hierarchically ordered porous nitrogen-doped carbon as a superior bifunctional electrocatalyst

Tingting Sun, Shu Zhao, Wenxing Chen, Dong Zhai, Juncai Dong, Yu Wang*, Shaolong Zhang, Aijuan Han, Lin Gu, Rong Yu, Xiaodong Wen, Hanlin Ren, Lianbin Xu, Chen Chen, Qing Peng, Dingsheng Wang*, and Yadong Li*

*Corresponding authors. wangyu@sinap.ac.cn (Y.W.); wangdingsheng@mail.tsinghua.edu.cn (D.W.); and ydli@mail.tsinghua.edu.cn (Y.L.)

www.pnas.org/cgi/doi/10.1073/pnas.1813605115

Table of Contents

1. Experimental Section

Chemicals. Triblock copolymer Pluronic F127 (M_w = 12.5K, PEO-PPO-PEO) was purchased from Sigma-Aldrich Co. Vitamin B12 (VB12) and 2,2-bipyridine were purchased from Shanghai Aladdin Biochemmical Technology Co., Ltd. Phenol (99%), sodium hydroxide (NaOH, 96%), formaldehyde solution (37%), tetraethoxysilane (TEOS, 98%), potassium hydroxide (KOH, 98%), ammonia solution ($NH_3 \cdot H_2O$, 28%), dicyandiamide (DCDA, 99%), and ethanol (99.7%) were obtained from Sinopharm Chemical. Iron (III) chloride hexahydrate ($FeCl_3 \cdot 6H_2O$, 97%), nickel (II) nitrate hexahydrate ($Ni(NO_3)_2 \cdot 6H_2O$, 98%), commercial 20 wt% Pt/C catalyst, and Nafion D-521 dispersion (5% w/w in water and 1-propanol) were purchased from Alfa Aesar (China) Chemicals Co., Ltd. Hydrofluoric acid (HF, 48-51%) was purchased from Acros Organics. Sulphuric acid (H_2SO_4, 98%) was purchased from Beijing Chemical Reagents. The distilled water used in all experiments was obtained through ion-exchange and filtration. All chemicals were used as received without further purification.

Synthesis of silica colloidal crystal (opal). Silica opal was prepared by published methods (1). Monodisperse silica spheres with a diameter of ca. 290 nm were initially prepared from hydrolysis of TEOS. The spheres were then formed into close-packed lattices through a sedimentation process over several months. This precipitate was then sintered at 120 ℃ for 2 days and then 750 ℃ for 4 hours, producing a robust opalescent piece that could be readily cut into smaller sections.

Synthesis of resol. Resol (M_w<500) was prepared by the method reported by Meng *et al*. previously (2). Specifically, 10 g phenol was melt at 40-42 ℃, then 2.13 g 20% NaOH aqueous solution was added dropwise over 10 min under stirring. Next, 17.7 g formaldehyde solution was added dropwise and the temperature was raised to 70 ℃. The mixture was heated and stirred for 60 min and then cooled to room temperature. After that, the pH of the solution was adjusted with 0.6 M HCl solution to neutral (7.0). Water was then removed under vaccum below 50 ℃. The synthesized resol was dissolved in ethanol before use.

Synthesis of Co-SAS/HOPNC. To prepare the Co-SAS/HOPNC catalyst, Pluronic F127 (1.0 g) and DCDA (1.0 g) were dispersed in ethanol (20 g) and deionized water (10 g) with magnetic stirring,

followed by adding a resol ethanol solution (20 wt%, 5.0 g). Next, VB12 (0.8 g) was dissolved into the above mixture and stirred at room temperature to produce a homogeneous pink solution. Subsequently, silica template (1.0 g) was soaked into the prepared precursor for 2 hours, and then kept at 50 ℃ in an electric oven for solvent evaporation for 8 h. After that, the impregnated composites were carried out from the solution and heated at 100 ℃ overnight for thermosetting. The pyrolysis process of the as-prepared composites was performed at 350 ℃ for 2 h and then 900 ℃ for 2 h in a tube furnace under Ar gas flowing with a ramping rate of 5 ℃ min^{-1}. Finally, the Co-SAS/HOPNC was produced by acid etching with diluted HF aqueous solution for 24 h to remove the silica opal. For comparative studies, a metal-free hierarchically ordered porous N-doped carbon (HOPNC) catalyst was synthesized by the same fabrication procedure as that for the Co-SAS/HOPNC but without adding VB12 in the precursor. The ordered macroporous N-doped carbon with single atomic Co sites (Co-SAS/OMNC) sample was synthesized through the same fabrication process as that for the Co-SAS/HOPNC but without adding F127 in the precursor. The Co nanoparticles (NPs) on the hierarchically ordered porous N-doped carbon (Co-NPs/HOPNC) sample was synthesized through the same preparation process as that for the Co-SAS/HOPNC but with adding more VB12 (2.0 g) in the precursor.

Electrochemical Tests. The HER electrochemical experiments were performed by a CHI 660E electrochemical workstation (Shanghai Chenhua Instrument Corp., China) in a three electrode cell with a catalyst covered glassy carbon rotating disk working electrode (5 mm in diameter), a Ag/AgCl (filled with 3.5 M KCl solution) reference electrode, and a graphite rod counter electrode. To prepare the catalyst ink, 5 mg catalyst powder was dispersed in 1.50 mL of DMF solution containing 40 μL of Nafion solution by sonication for at least 1 h. Then a certain volume of the catalyst ink was spread on the surface of glassy carbon electrode with the nonprecious catalyst loading was 0.6 mg cm^{-2} and the loading of 20 wt% Pt/C was 0.12 mg cm^{-2} and then dried under room temperature. For the Pt/C catalyst with the mass loading of 0.12 mg cm^{-2}, the Pt loading is 24 μg_{Pt} cm^{-2}. For the Co-SAS/HOPNC catalyst with the mass loading of 0.6 mg cm^{-2}, the Co loading is merely 2.9 μg_{Co} cm^{-2} based on the ICP-OES analysis. All the potentials were quoted against the reversible hydrogen electrode (RHE). For the ORR catalytic performance test, O_2-purged 0.1 M KOH or 0.1 M $HClO_4$ was used as the electrolyte. The RDE measurements were carried out under the rotation rates ranging from 400 to 2500 rpm at a scan rate of 5 mV s^{-1}. For the HER catalytic performance test, Ar gas flow was carried out through the electrolyte (0.5 M H_2SO_4 or 0.1 M KOH) during the electrochemical measurements. Linear sweep voltammetry was measured at a scan rate of 5 mV s^{-1} with an electrode rotation speed of 1600 rpm. Electrochemical impedance spectroscopy (EIS) analysis was performed at -0.1 V vs. RHE in the frequency range from 10 kHz to 0.01 Hz using an amplitude of 5 mV.

Synthesis of Fe-SAS/HOPNC. 1.0 g F127 and 1.86 g 2,2-bipyridine were first dissolved in a

mixture of 20 g ethanol and 10 g water under continuous stirring for 30 min. 5.0 g of resol ethanol solution (20 wt%) was then added and stirred for another 30 min. Next, 0.45 g $FeCl_3$ $6H_2O$ was added into the solution under stirring. Subsequently, silica template (1.0 g) was soaked into the prepared precursor for 2 hours, and then kept at 50 ℃ in an electric oven for solvent evaporation for 8 h. After that, the impregnated composites were carried out from the solution and heated at 100 ℃ overnight for thermosetting. The resulting composites were then heated under Ar atmosphere at 350 ℃ for 2 h at a heating rate of 2 ℃ min^{-1}, and at 5 ℃ min^{-1} rising to 600 ℃, followed by a 2 h soak for further carbonation. Finally, the freestanding Fe-SAS/HOPNC was obtained by removing the silica opal with a 5 wt% HF solution (24 h).

Synthesis of Ni-SAS/HOPNC. 1.0 g F127 and 1.5 g DCDA were first dissolved in a mixture of 20 g ethanol and 10 g water under continuous stirring for 30 min. 5.0 g of resol ethanol solution (20 wt%) was then added and stirred for another 30 min. Next, 0.32 g $Ni(NO_3)_2$ $6H_2O$ was added into the solution under stirring. Subsequently, silica template (1.0 g) was soaked into the prepared precursor for 2 hours, and then kept at 50 ℃ in an electric oven for solvent evaporation for 8 h. After that, the impregnated composites were carried out from the solution and heated at 100 ℃ overnight for thermosetting. The resulting composites were then heated under Ar atmosphere at 350 ℃ for 2 h at a heating rate of 2 ℃ min^{-1}, and at 5 ℃ min^{-1} rising to 600 ℃, followed by a 2 h soak for further carbonation. Finally, the freestanding Ni-SAS/HOPNC was obtained by removing the silica opal with a 5 wt% HF solution (24 h).

Physicochemical characterization. Powder X-ray diffraction patterns of samples were recorded using a Rigaku RU-200b X-ray powder diffractometer (XRD) with Cu Kα radiation (λ = 1.5406 Å). TEM images were performed on a Hitachi H-800 transmission electron microscope. The high-resolution TEM (HR-TEM), high-angle annular dark-field scanning transmission electron microscopy (HAADF-STEM) images and elemental mapping were recorded on a JEOL-2100F FETEM with electron acceleration energy of 200 kV. The scanning electron microscope (SEM) was carried out by a JSM-6700F SEM. Photoemission spectroscopy experiments (XPS) were performed at the Catalysis and Surface Science End station at the BL11U beamline of National Synchrotron Radiation Laboratory (NSRL) in Hefei, China. Elemental analysis of Co in the solid samples was detected by an Optima 7300 DV inductively coupled plasma atomic emission spectrometer (ICP-AES).

XAFS measurement and analysis. *Ex situ* and *in situ* XAFS spectra at the Co K-edge (7709 eV) was measured at BL14W1 station in Shanghai Synchrotron Radiation Facility (SSRF). The Co K-edge XAFS data were recorded in a fluorescence mode. Co foil, CoO, and Co_3O_4 were used as references. All spectra were collected in ambient conditions.

The acquired EXAFS data were processed according to the standard procedures using the ATHENA

module implemented in the IFEFFIT software packages. The k^3-weighted EXAFS spectra were obtained by subtracting the post-edge background from the overall absorption and then normalizing with respect to the edge-jump step. Subsequently, k^3-weighted $\chi(k)$ data of Co K-edge were Fourier transformed to real (R) space using a hanning windows (dk=1.0 $Å^{-1}$) to separate the EXAFS contributions from different coordination shells. To obtain the quantitative structural parameters around central atoms, least-squares curve parameter fitting was performed using the ARTEMIS module of IFEFFIT software packages.

The following EXAFS equation was used:

$$\chi(k) = \sum_j \frac{N_j S_0^2 F_j(k)}{k R_j^2} \exp[-2k^2\sigma_j^2] \exp[\frac{-2R_j}{\lambda(k)}] \sin[2kR_j + \phi_j(k)]$$

S_0^2 is the amplitude reduction factor, $F_j(k)$ is the effective curved-wave backscattering amplitude, N_j is the number of neighbors in the j^{th} atomic shell, R_j is the distance between the X-ray absorbing central atom and the atoms in the j^{th} atomic shell (backscatterer), λ is the mean free path in Å, $\phi_j(k)$ is the phase shift (including the phase shift for each shell and the total central atom phase shift), σ_j is the Debye-Waller parameter of the j^{th} atomic shell (variation of distances around the average R_j). The functions $F_j(k)$, λ and $\phi_j(k)$ were calculated with the ab initio code FEFF8.2. The additional details for EXAFS simulations are given below.

The coordination numbers of model samples were fixed as the nominal values. The obtained S_0^2 was fixed in the subsequent fitting. While the internal atomic distances R, Debye-Waller factor σ^2, and the edge-energy shift ΔE_0 were allowed to run freely.

For in situ spectroscopic experiments, a homemade electrochemical cell was used and the spectra were collected using a solid-state detector. A catalyst-coated carbon fiber paper (Co-SAS/HOPNC/CFP) working electrode served as the X-ray window for synchrotron radiation, and multistep potential control was used for the in situ measurements.

Calculation of electron transfer numbers (n) and kinetic currents (J_k) for ORR. The n and J_k involved in the typical ORR process were calculated on the basis of the Koutecky-Levich equation:

$$\frac{1}{J} = \frac{1}{J_k} + \frac{1}{J_d} = \frac{1}{J_k} + \frac{1}{B\omega^{1/2}}$$

$$B = 0.62nFC_o(D_o)^{2/3}v^{-1/6}$$

where J is the measured current density, J_k and J_d are the kinetic-limiting and diffusion-limiting current densities, ω is the rotation speed in rpm, n is the electron transfer number, F is the Faraday constant (96485 C mol^{-1}), D_o is the diffusion coefficient of oxygen in the electrolyte (1.9×10^{-5} cm^2 s^{-1}), v is the kinetic viscosity of the electrolyte (0.01 cm^2 s^{-1}), and C_o is the bulk concentration of oxygen (1.2×10^{-6} mol cm^{-3}).

Calculation of turnover frequency (TOF) for HER. To calculate the turnover frequency (TOF) per cobalt site on the Co-SAS/HOPNC catalyst, we used the following formula:

$$\text{TOF} = \frac{\#\ \text{total hydrogen turnover / cm}^2\ \text{geometric area}}{\#\ \text{active sites / cm}^2\ \text{geometric area}}$$

The upper limit of the number of active sites was calculated based on the hypothesis that all cobalt atoms in the Co-SAS/HOPNC catalyst formed active Co-N_4 centers and all of them were accessible to the electrolyte. The real number of active and accessible cobalt sites should be considerably lower than the calculated value. The cobalt content of Co-SAS/HOPNC revealed by the ICP-OES measurement was 0.49 wt%. Accordingly, the upper limit of active site density is

$$\frac{0.49}{100}\frac{\text{mg}}{\text{mg}} \times 0.60\frac{\text{mg}}{\text{cm}^2} \times \frac{1}{58.93}\frac{\text{mmol}}{\text{mg}} \times 6.022 \times 10^{20}\ \frac{\text{sites}}{\text{mmol}} = 3.0 \times 10^{16}\ \text{sites cm}^{-2}$$

The total number of hydrogen turn overs was calculated from the current density according to (3, 4):

$$\#\ H_2 = (j\frac{\text{mA}}{\text{cm}^2})(\frac{1\text{C/s}}{1000\ \text{mA}})(\frac{1\text{mol e}^-}{96485.3\text{C}})(\frac{1\text{mol H}_2}{2\text{mol e}^-})(\frac{6.02 \times 10^{23}\ \text{molecules H}_2}{1\text{mol H}_2}) = 3.12 \times 10^{15}\ \frac{\text{H}_2/\text{s}}{\text{cm}^2}\text{per}\frac{\text{mA}}{\text{cm}^2}$$

For example, at an overpotential of 100 mV, the HER current density is 3.95 mA cm^{-2}, and the TOF of the Co-SAS/HOPNC was calculated to be

$$\text{TOF} = \frac{3.12\times 10^{15}\times \frac{\text{H}_2/\text{s}}{\text{cm}^2}\text{per}\frac{\text{mA}}{\text{cm}^2} \times 3.95\frac{\text{mA}}{\text{cm}^2}}{3.0 \times 10^{16}\ \text{sites cm}^{-2}} = 0.41\ \text{s}^{-1}$$

The TOF of the Co-SAS/HOPNC at the overpotential of 200 mV was calculated to be

$$\text{TOF} = \frac{3.12\times 10^{15}\times \frac{\text{H}_2/\text{s}}{\text{cm}^2}\text{per}\frac{\text{mA}}{\text{cm}^2} \times 36.5\frac{\text{mA}}{\text{cm}^2}}{3.0 \times 10^{16}\ \text{sites cm}^{-2}} = 3.8\ \text{s}^{-1}$$

The cobalt content of Co-SAS/OMNC revealed by the ICP-OES measurement was 0.42 wt%. Accordingly, the upper limit of active site density is

$$\frac{0.42}{100}\frac{\text{mg}}{\text{mg}} \times 0.60\frac{\text{mg}}{\text{cm}^2} \times \frac{1}{58.93}\frac{\text{mmol}}{\text{mg}} \times 6.022 \times 10^{20}\ \frac{\text{sites}}{\text{mmol}} = 2.57 \times 10^{16}\ \text{sites cm}^{-2}$$

Similarly, the TOF of the Co-SAS/OMNC at the overpotential of 200 mV was calculated to be

$$\text{TOF} = \frac{3.12\times 10^{15}\times \frac{\text{H}_2/\text{s}}{\text{cm}^2}\text{per}\frac{\text{mA}}{\text{cm}^2} \times 8.5\frac{\text{mA}}{\text{cm}^2}}{2.57 \times 10^{16}\ \text{sites cm}^{-2}} = 1.03\ \text{s}^{-1}$$

2. DFT calculations

All theoretical calculations were performed using density functional theory (DFT), as implemented in the Vienna ab initio simulation package (VASP) (5, 6). The electron exchange and correlation energy was treated within the generalized gradient approximation in the Perdew-Burke-Ernzerhof functional (GGA-PBE) (7). The valence orbitals of Co (3d, 4s), C (2s, 2p), N (2s, 2p) and H (1s) were described by plane-wave basis sets with cutoff energies of 400 eV. The k-point sampling was obtained from the Monkhorst-Pack scheme with a ($2 \times 2 \times 1$) mesh. The convergence criteria for the electronic self-consistent iteration and force were set to 10^{-4} eV and 0.03 eV $Å^{-1}$, respectively. For evaluating the energy barriers, all transition states were located using the climbing image nudged elastic band (CI-NEB) method (8-10).

The two-dimensional system was modeled with a 6×6 supercell consisted of 72 carbon sites separated by a vacuum region of 15 Å along the direction normal to the sheet plane to avoid strong interactions between two adjacent layers. Two neighboring carbon atoms were removed to anchor a Co atom, and four of carbon atoms were replaced by N atom, forming the Co-N_4-C configuration (See Fig. S28). A *p* (2×2) four-atomic-layer slab model of fcc Co (111) surface was used to simulate the electrocatalytic reactivity of Co nanoparticle. The vacuum gap was set as 15 Å and the top two layers were relaxed. The charge density differences were evaluated using the formula $\Delta\rho = \rho A + B - \rho A - \rho B.$, where ρX is the electron density of X.

For ORR calculation, the four electron pathway by which the ORR occurs under base condition are generally reported to proceed according to the following steps (11):

(1) $* + O_2\,(g) + H_2O\,(l) + e^- \rightarrow *OOH + OH^-$

(2) $*OOH + e^- \rightarrow *O + OH^-$

(3) $*O + H_2O\,(l) + e^- \rightarrow *OH + OH^-$

(4) $*OH + e^- \rightarrow OH^- + *$

where the asterisk (*) indicates an active site.

We used Nørskov *et al.*'s computational hydrogen electrode model to calculate the free energy diagrams for ORR (12). The reaction free energy (G) can be calculated by the formula:

$$G = \Delta H - T\Delta S - qU,$$

where ΔH is the reaction enthalpy of an elementary step in ORR and is estimated by the reaction energy (ΔE) from DFT calculations with zero-point energy (ZPE) correction; $T\Delta S$ is the change in entropy contribution to the free energy; U is the applied potential; q is the charge transfer in each elementary step. Zero-pint energy (ZPE) and entropy contribution (T*S) for adsorbed species and gaseous molecules (H_2O and H_2) were obtained using harmonic approximation and ideal gas approximation, respectively, at the standard condition. The calculated ZPE and T*S are listed in Tables S7 and S8. The free energy of H_2O (l) was derived from the equation $G(H_2O, l) = G(H_2O, g)$

+ $RT\ln(p/p_0)$, where R is the ideal gas constant, T = 298.15 K, p = 0.035 bar, and p_0 = 1 bar.

The free energy of OH^- was derived from the following equations:

$$G(OH^-) = G(H_2O, l) - G(H^+)$$

$$G(H^+) = 0.5G(H_2) - k_BT\ln10 \times pH$$

where k_B is the Boltzmann's constant, T = 298.15 K, and pH = 13.

The free energy of O_2 was obtained from the reaction O_2 (g) + $2H_2$ (g) → $2H_2O$ (l), with a known free energy decrease of 4.92 eV.

For HER calculation, the hydrogen adsorption energies were calculated according to the equation:

$$\Delta E_H = E(H/substrate) - [E(substrate) + 1/2\ E(H_2)]$$

where E(H/substrate), E(substrate) and $E(H_2)$ represent the total energy of substrate with adsorbed hydrogen atom, the total energy of the clean substrate and the energy of H_2 molecule in the gas phase, respectively. The Gibbs free energy of hydrogen adsorption can be calculated by the equation:

$$\Delta G_H = \Delta E_H + \Delta E_{ZPE} + \Delta H_H - T\Delta S_H$$

where ΔE_H, ΔE_{ZPE}, ΔH_H and ΔS_H denote the adsorption energy, zero point energy change, enthalpy change from 0 to 298 K, and entropy change between the adsorbed state and the gas phase, respectively. Since the energy contribution from the configurational and vibrational entropy in the hydrogen-adsorbed substrate could be neglected, ΔS_H was determined by $\Delta S_H = -1/2S_{H_2}$, where S_{H_2} is the entropy of molecule hydrogen in the gas phase at standard conditions (13).

3. References

1. Zakhidov AA, et al. (1998) Carbon structures with three-dimensional periodicity at optical wavelengths. *Science* 282:897–901.
2. Meng Y, et al. (2005) Ordered mesoporous polymers and homologous carbon frameworks: Amphiphilic surfactant templating and direct transformation. *Angew Chem Int Ed Engl* 44:7053–7059.
3. Liang HW, et al. (2015) Molecular metal-N_x centres in porous carbon for electrocatalytic hydrogen evolution. *Nat Commun* 6:7992.
4. Kibsgaard J, Jaramillo TF (2014) Molybdenum phosphosulfide: An active, acid-stable, earth-abundant catalyst for the hydrogen evolution reaction. *Angew Chem Int Ed Engl* 53:14433–14437.
5. Kresse G, Furthmüller J (1996) Efficiency of ab-initio total energy calculations for metals and semiconductors using a plane-wave basis set. *Comp Mater Sci 6*:15–50.
6. Kresse G, Furthmüller J (1996) Efficient iterative schemes for ab *initio* total-energy calculations using a plane-wave basis set. *Phys Rev B* 54:11169–11186.
7. Perdew JP, Burke K, Ernzerhof M (1996) Generalized gradient approximation made simple. *Phys Rev Lett* 77:3865–3868.
8. Hinnemann B, et al. (2005) Biomimetic hydrogen evolution: MoS_2 nanoparticles as catalyst for hydrogen evolution. *J Am Chem Soc* 127:5308–5309.
9. Jónsson H, Mills G, Jacobsen KW (1998) Classical and quantum dynamics in condensed phase simulations. *Nudged Elastic Band Method for Finding Minimum Energy Paths of Transitions*, eds Berne B, Ciccoti G, Coker DF (World Scientific, Hackensack, NJ), pp 385–404.
10. Henkelman G, Uberuaga BP, Jónsson H (2000) A climbing image nudged elastic band method for finding saddle points and minimum energy paths. *J Chem Phys* 113:9901–9904.
11. Jiao Y, Zheng Y, Jaroniec M, Qiao SZ (2015) Design of electrocatalysts for oxygen- and hydrogen-involving energy conversion reactions. *Chem Soc Rev* 44:2060–2086.
12. Nørskov JK, et al. (2004) Origin of the overpotential for oxygen reduction at a fuel-cell cathode. *J Phys Chem B* 108:17886–17892.
13. Henkelman G, Jónsson H (2000) Improved tangent estimate in the nudged elastic band method for finding minimum energy paths and saddle points. *J Chem Phys* 113:9978–9985.

4. Supplementary Figures and Tables

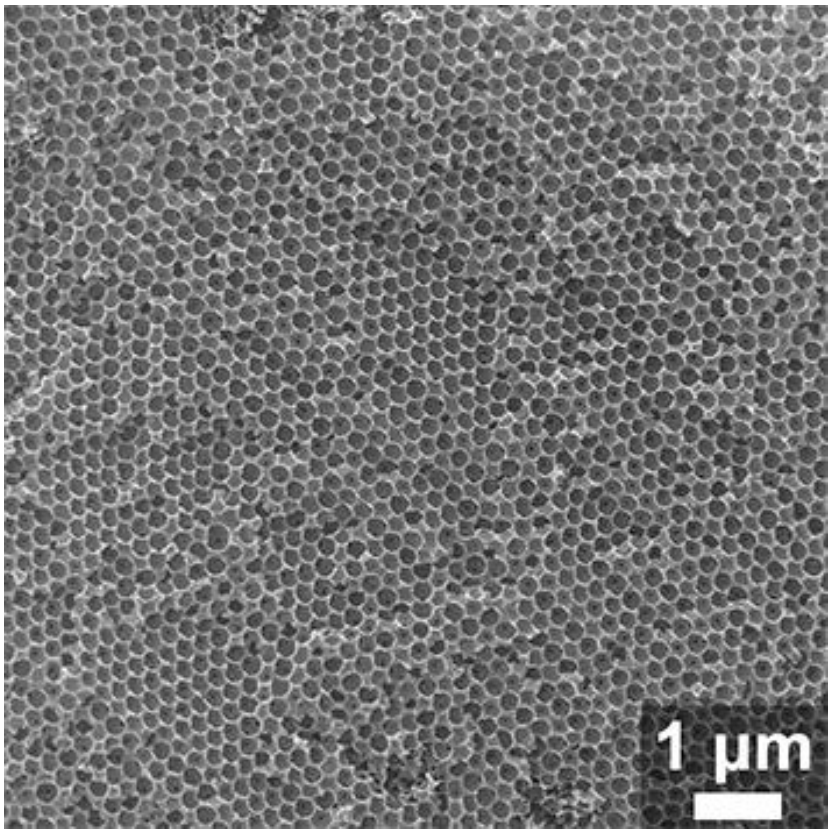

Fig. S1. SEM image of the Co-SAS/HOPNC.

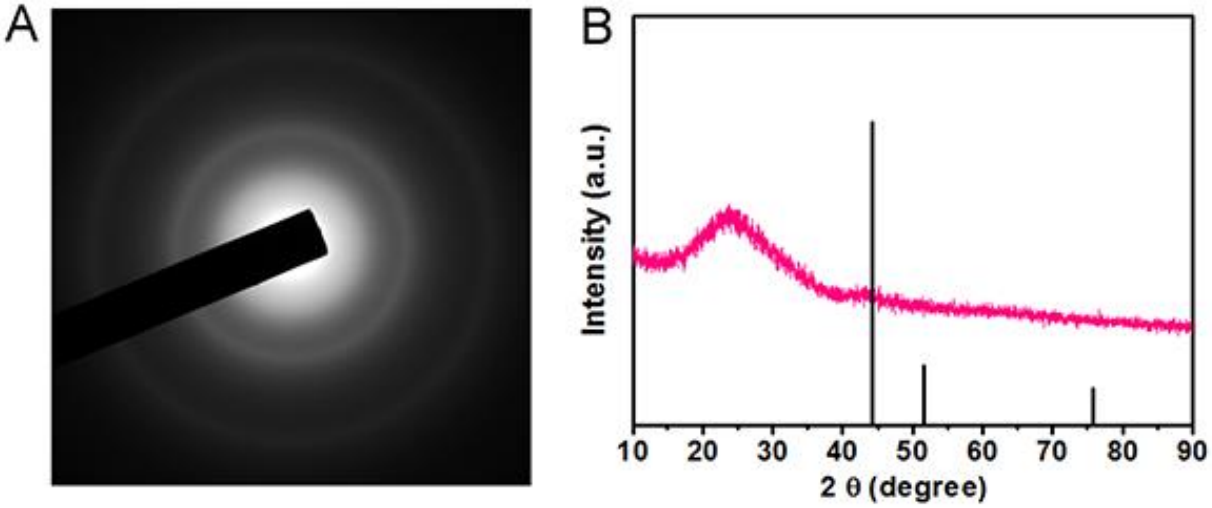

Fig. S2. (*A*) SAED pattern of Co-SAS/HOPNC. (*B*) XRD patterns of Co-SAS/HOPNC with Co (JCPDS No. 15-0806, black vertical line) as reference.

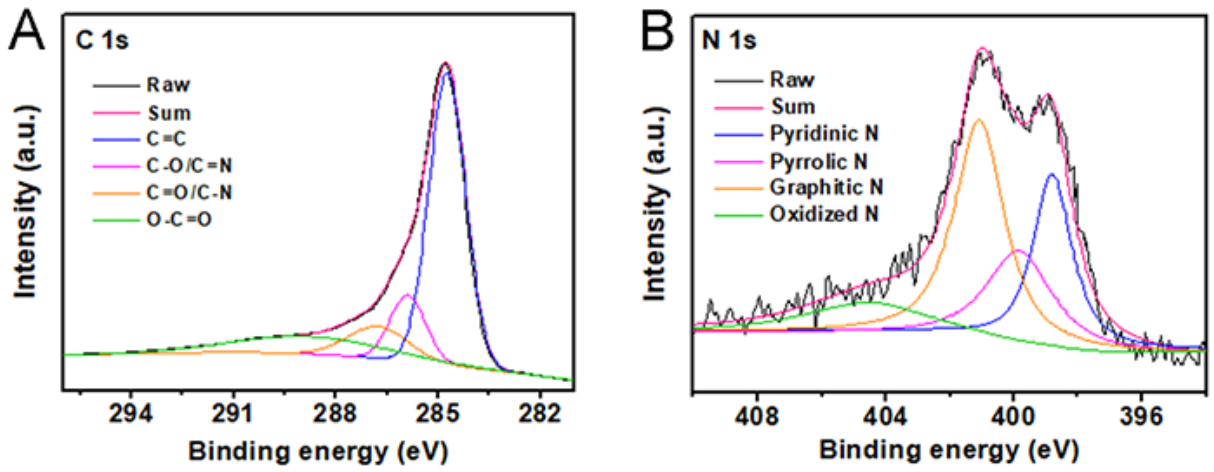

Fig. S3. (*A*) C 1s and (*B*) N 1s XPS spectra of Co-SAS/HOPNC.

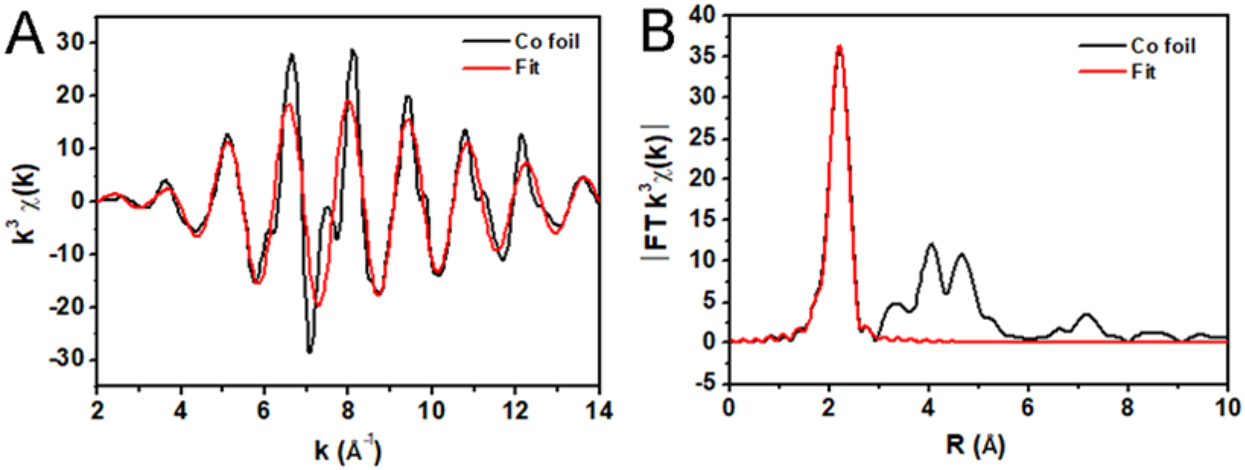

Fig. S4. The corresponding EXAFS fitting curves of Co foil.

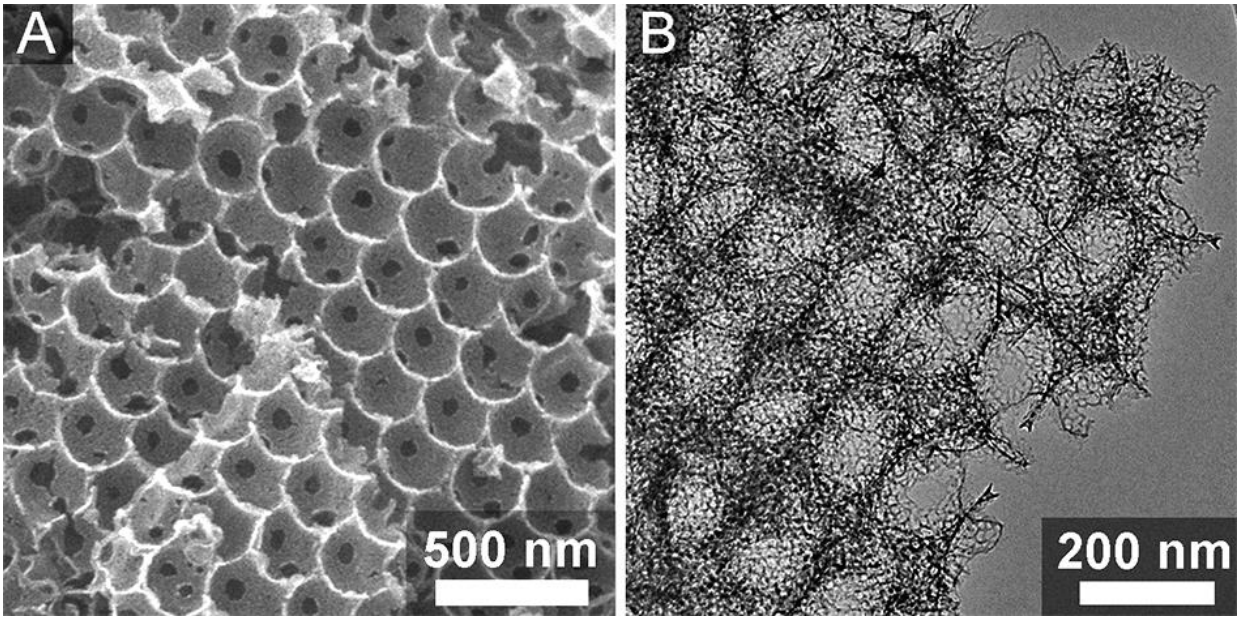

Fig. S5. (*A*) SEM and (*B*) TEM images of HOPNC.

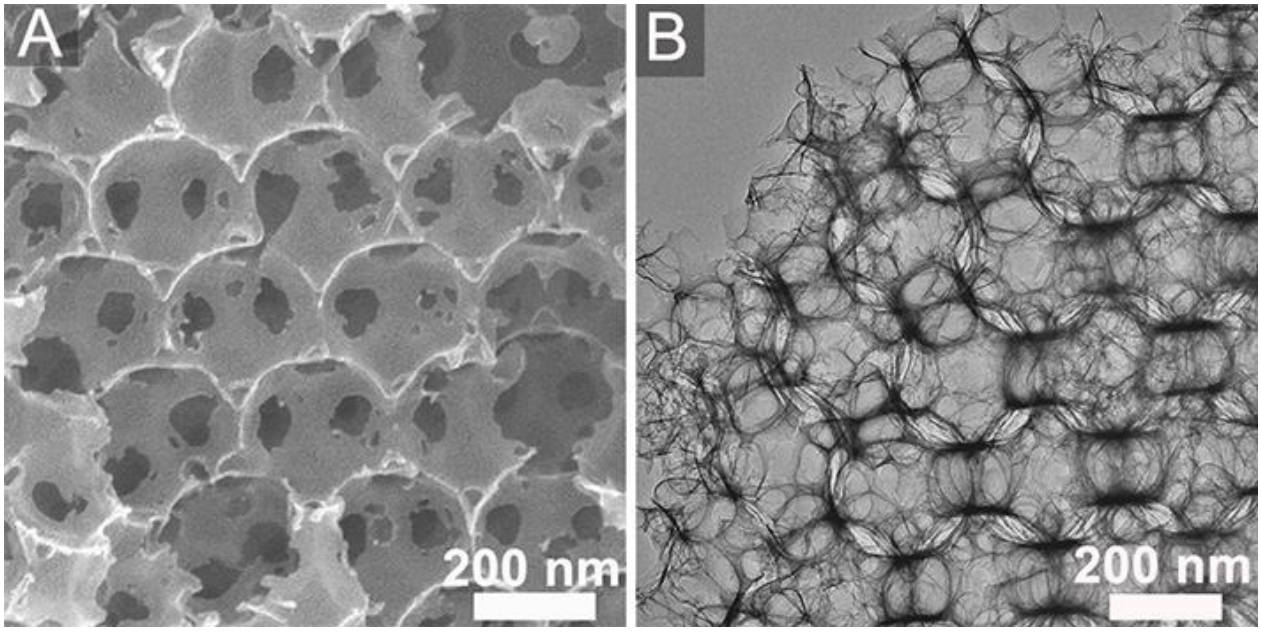

Fig. S6. (*A*) SEM and (*B*) TEM images of Co-SAS/OMNC.

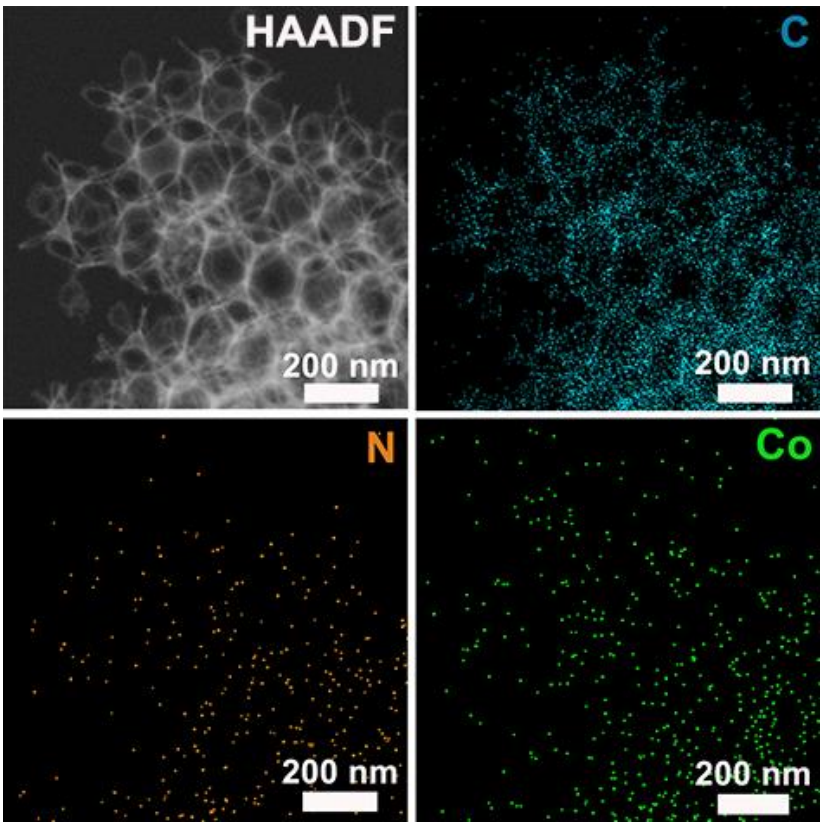

Fig. S7. HAADF-STEM image of Co-SAS/OMNC and corresponding element maps showing the distribution of C (blue), N (orange), and Co (green).

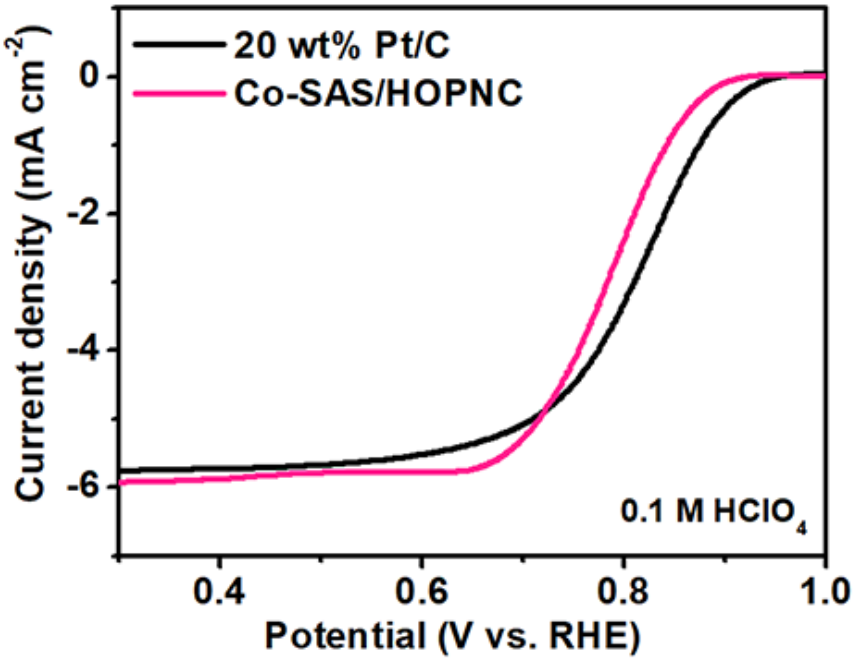

Fig. S8. ORR LSV curves for the Co-SAS/HOPNC and 20 wt% Pt/C catalysts in 0.1 M $HClO_4$ at the rotating rate of 1600 rpm (scan rate: 5 mV s^{-1}).

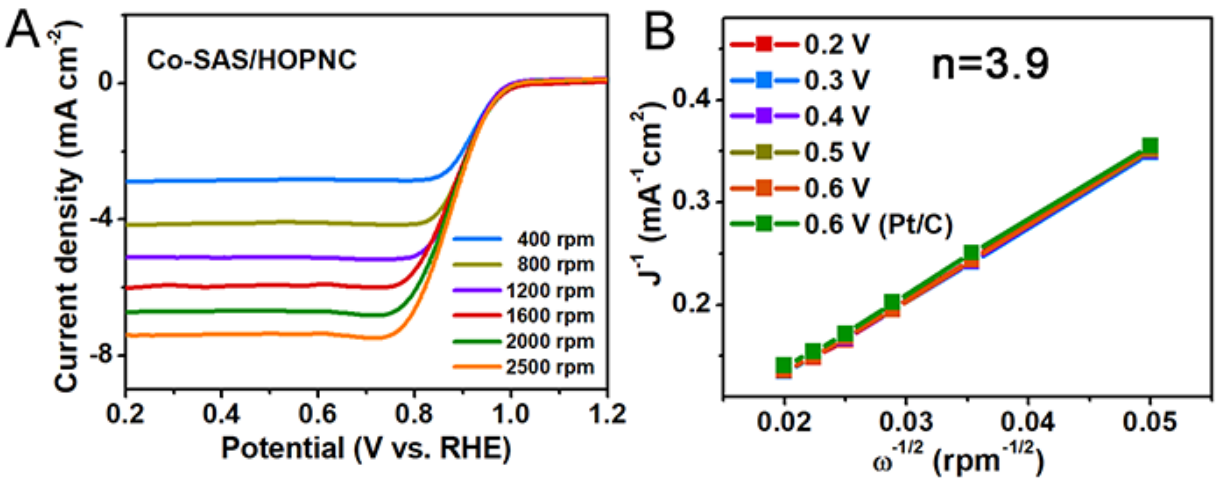

Fig. S9. (*A*) ORR LSV curves of Co-SAS/HOPNC in O_2-saturated 0.1 M KOH at various rotating rates (400-2500 rpm). (*B*) K–L plots of Co-SAS/HOPNC and Pt/C at different potentials.

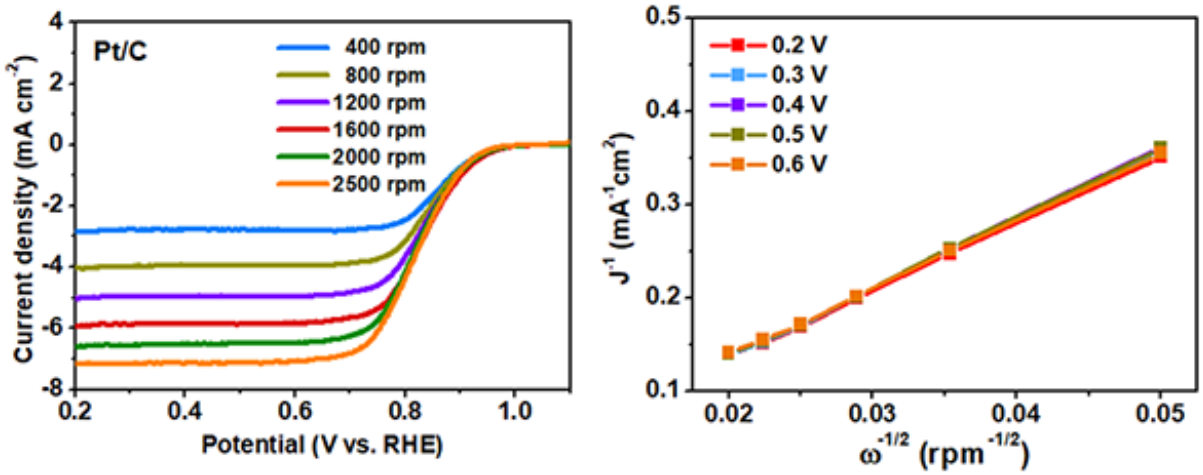

Fig. S10. LSV curves of 20 wt% Pt/C in O_2-saturated 0.1 M KOH at 400-2500 rpm and the corresponding K–L plots at various potentials.

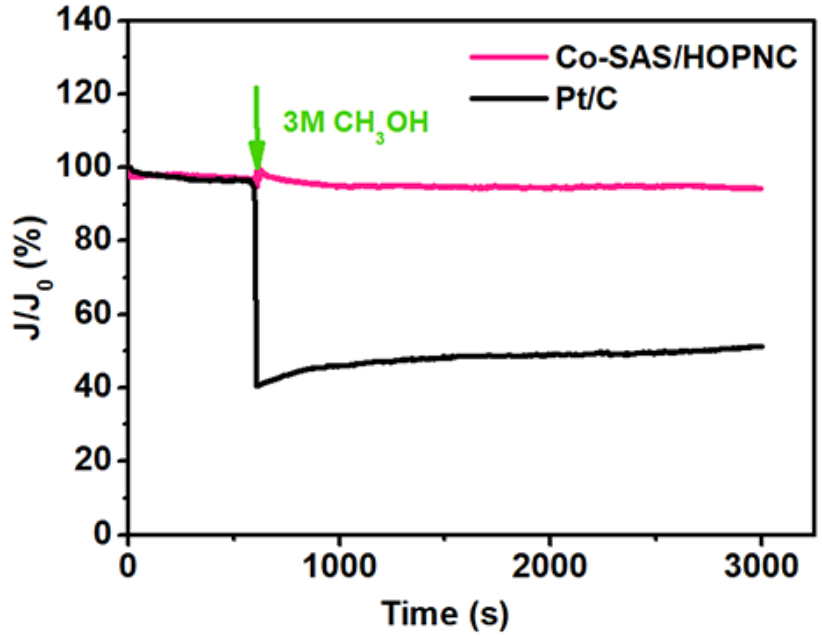

Fig. S11. The stability evaluation for Co-SAS/HOPNC and Pt/C catalysts in O_2-saturated 0.1 M KOH with the injection of 3 M methanol.

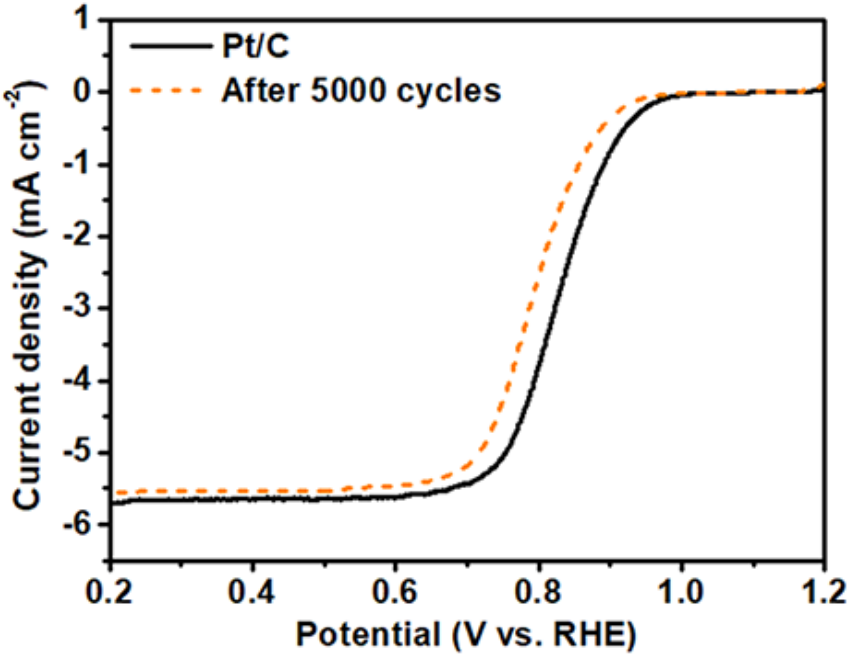

Fig. S12. ORR LSV curves of Pt/C initially and after 5000 cycles between 0.5 and 1.0 V at a scan rate 100 mV s^{-1}.

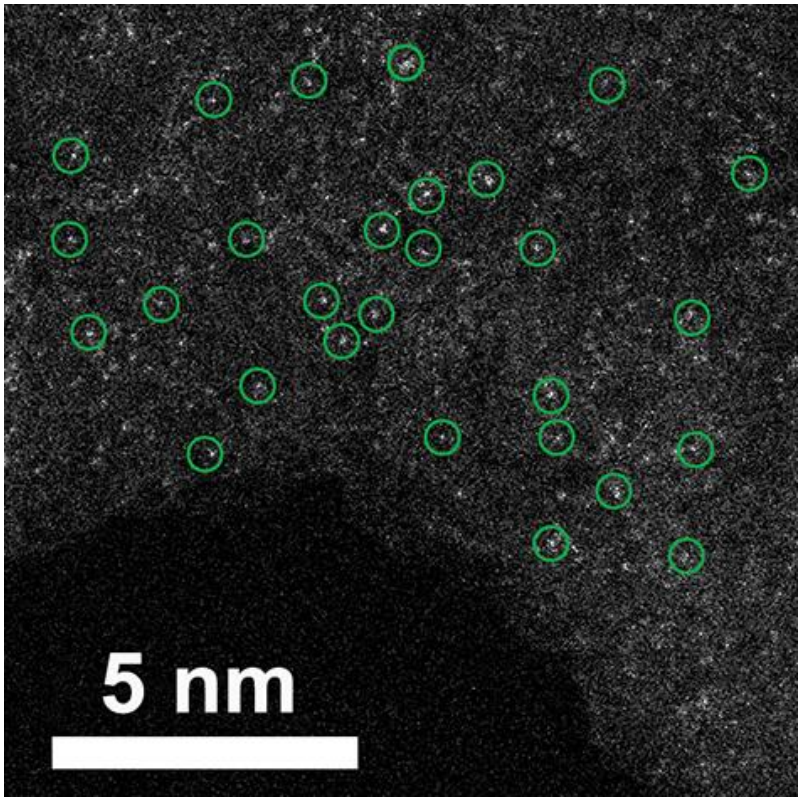

Fig. S13. AC HAADF-STEM image of Co-SAS/HOPNC after 5000 CV cycles in 0.1 M KOH for ORR.

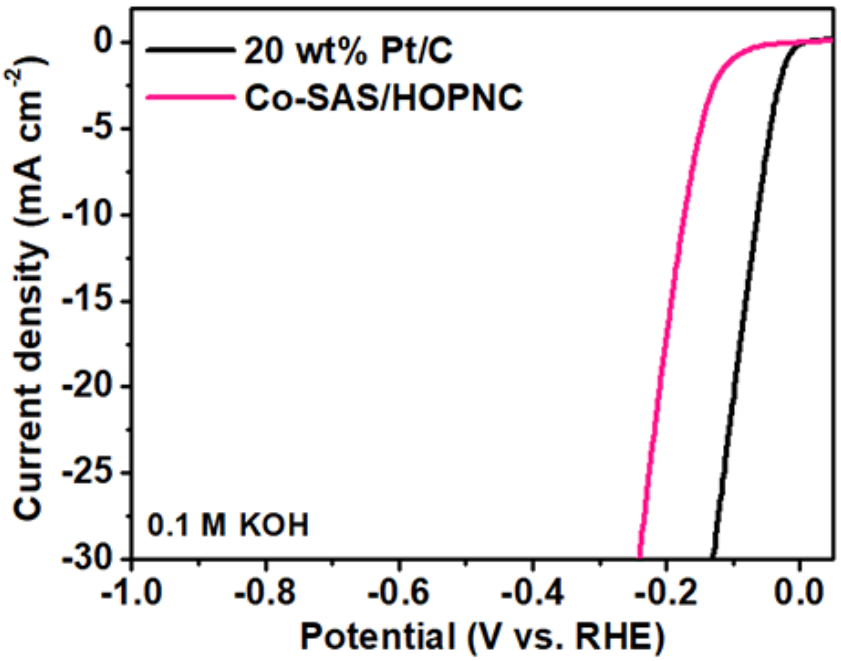

Fig. S14. HER polarization curves for the Co-SAS/HOPNC and 20 wt% Pt/C in 0.1 M KOH at the rotating rate of 1600 rpm (scan rate: 5 mV s^{-1}).

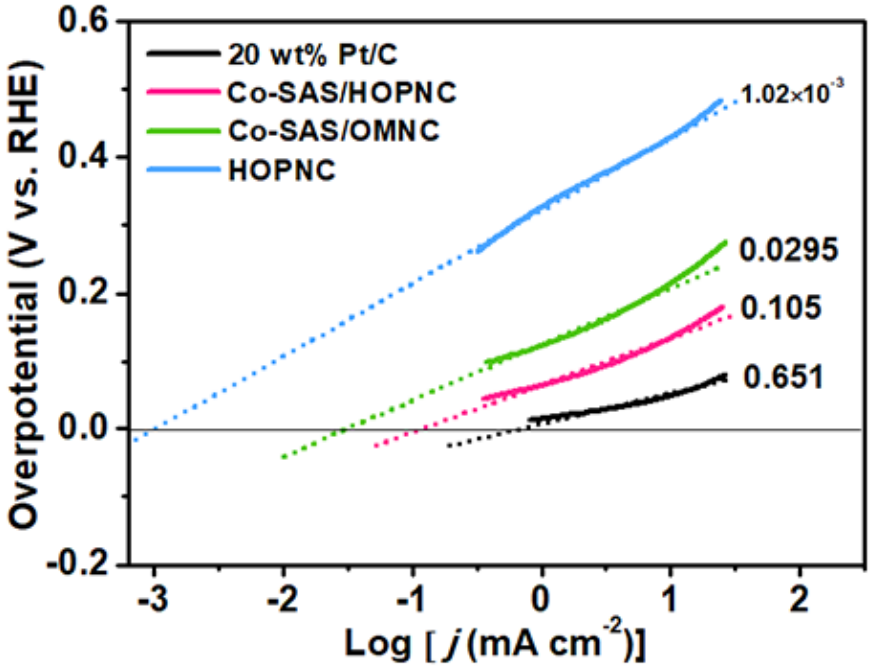

Fig. S15. The exchange current density for the catalysts tested in 0.5 M H_2SO_4.

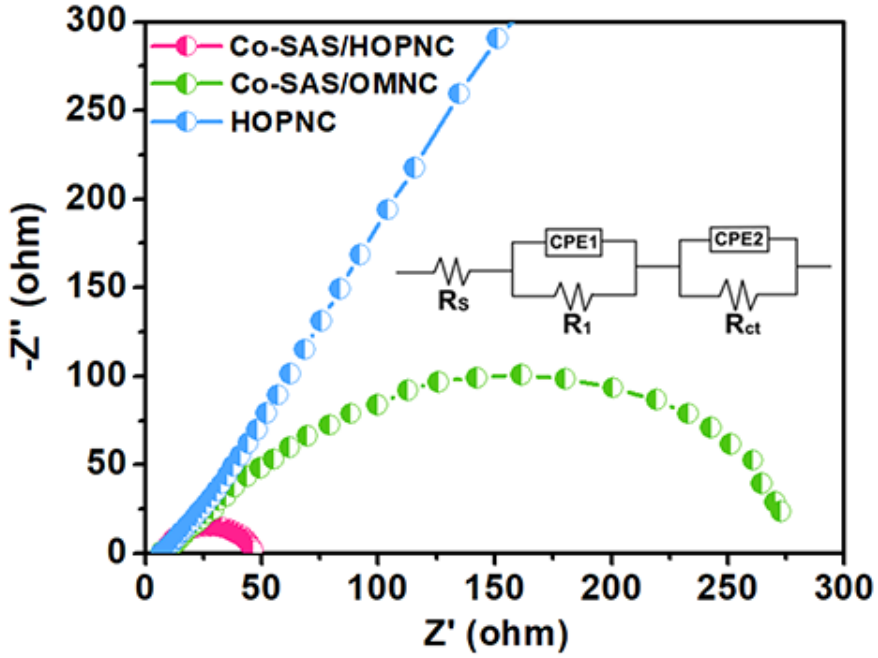

Fig. S16. Nyquist plots of the Co-SAS/HOPNC, Co-SAS/OMNC, and HOPNC, inset: equivalent circuit model applied to fit the Nyquist plots, where R_s is the series resistance, R_{ct} is the charge transfer resistance, R_1 relates to the interfacial resistance resulting from the electron transport between the catalyst and the GCE, and CPE1 and CPE2 represent the double layer capacitance.

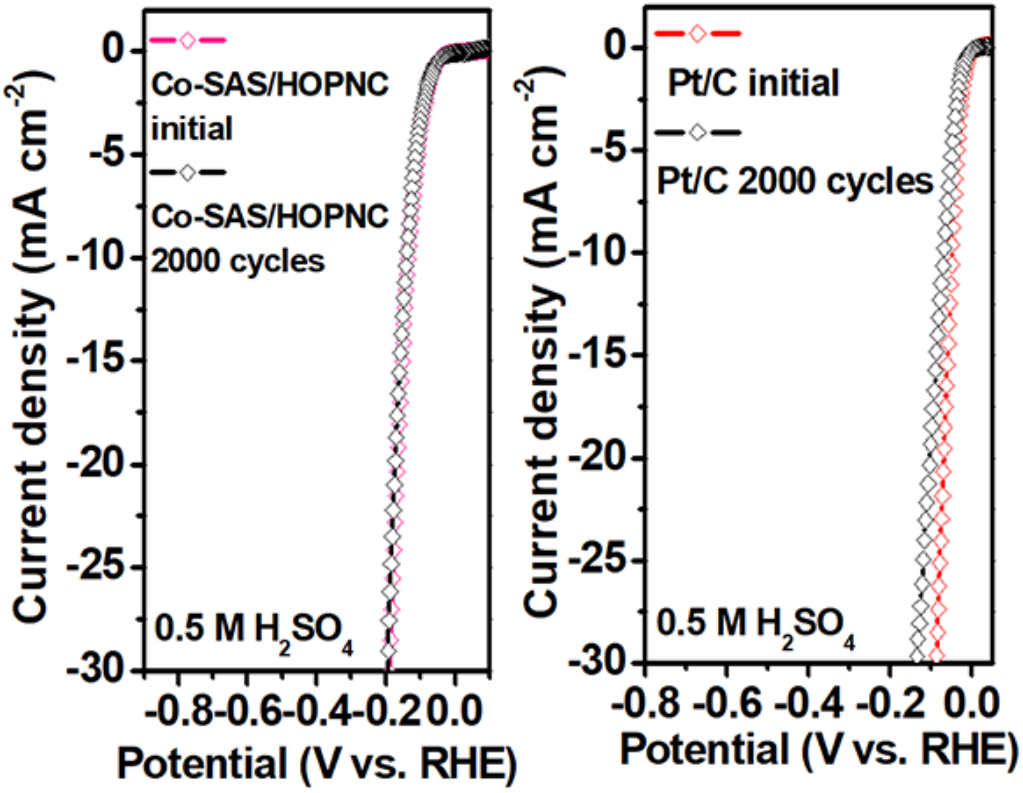

Fig. S17. Polarization curves of Co-SAS/HOPNC and Pt/C initially and after 2000 CV sweeps between -0.3 and 0.2 V vs. RHE.

Fig. S18. *In situ* XAS device, CE, RE, and WE represent counter, reference, and working electrodes, respectively.

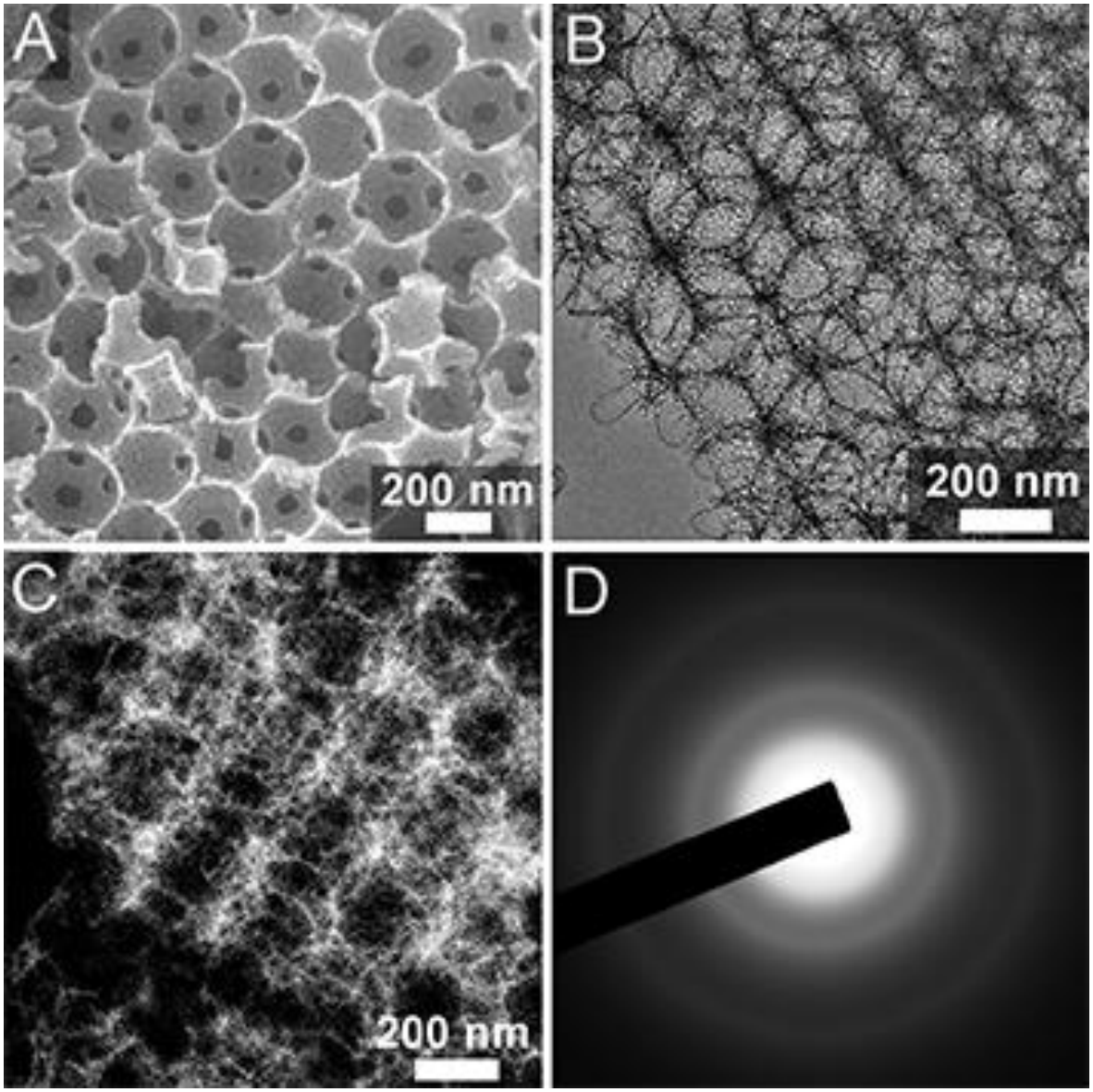

Fig. S19. (*A*) SEM, (*B*) TEM, (*C*) STEM images, and (*D*) electron diffraction pattern of Co-SAS/HOPNC after 2000 CV cycles in 0.5 M H_2SO_4 for HER. We found that the Co-SAS/HOPNC still maintained ordered porous structure. Small particles of Co species are not observed.

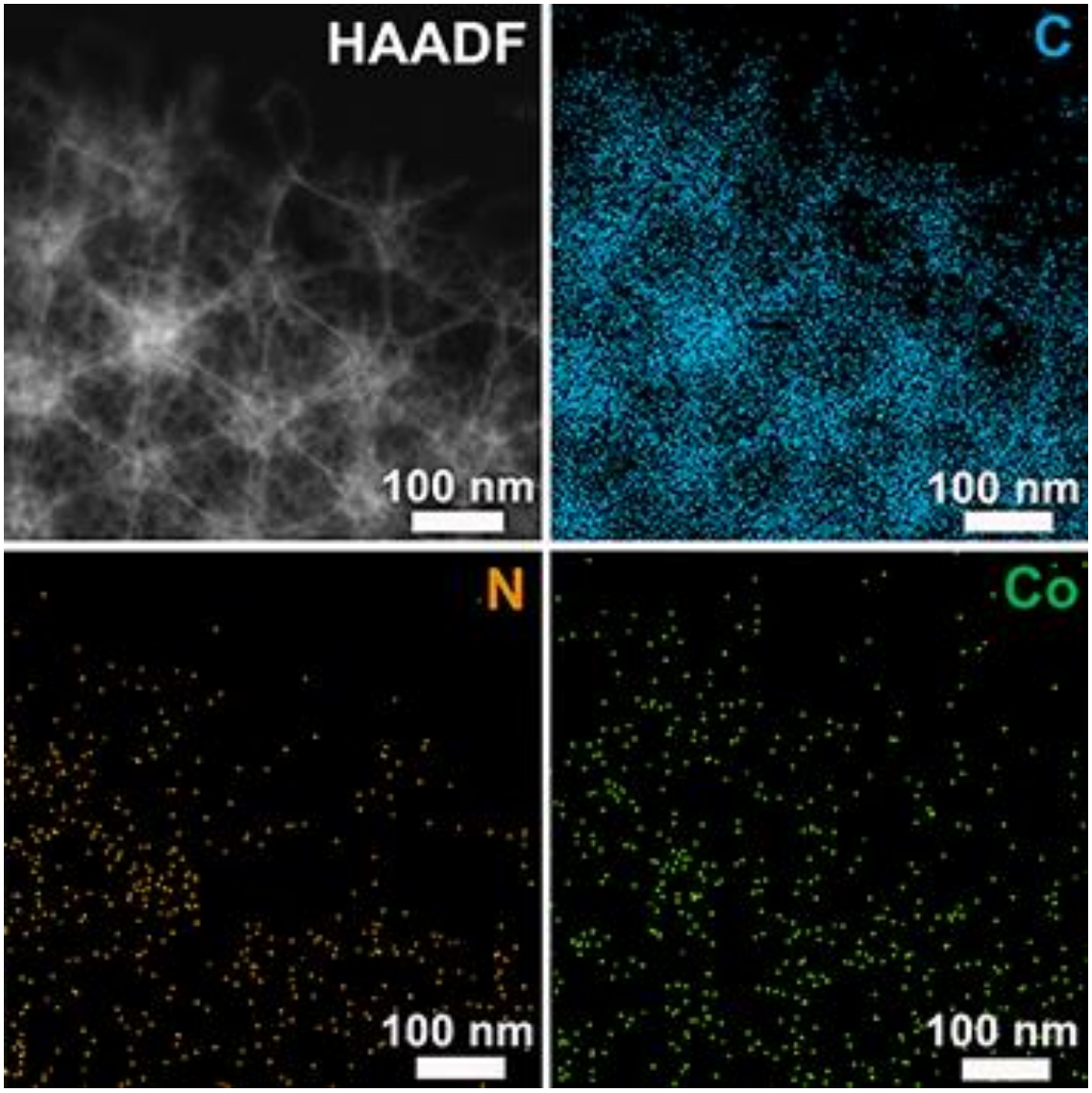

Fig. S20. HAADF-STEM image of Co-SAS/HOPNC after 2000 CV cycles in 0.5 M H_2SO_4 for HER and corresponding element maps showing the distribution of C (blue), N (orange), and N (green).

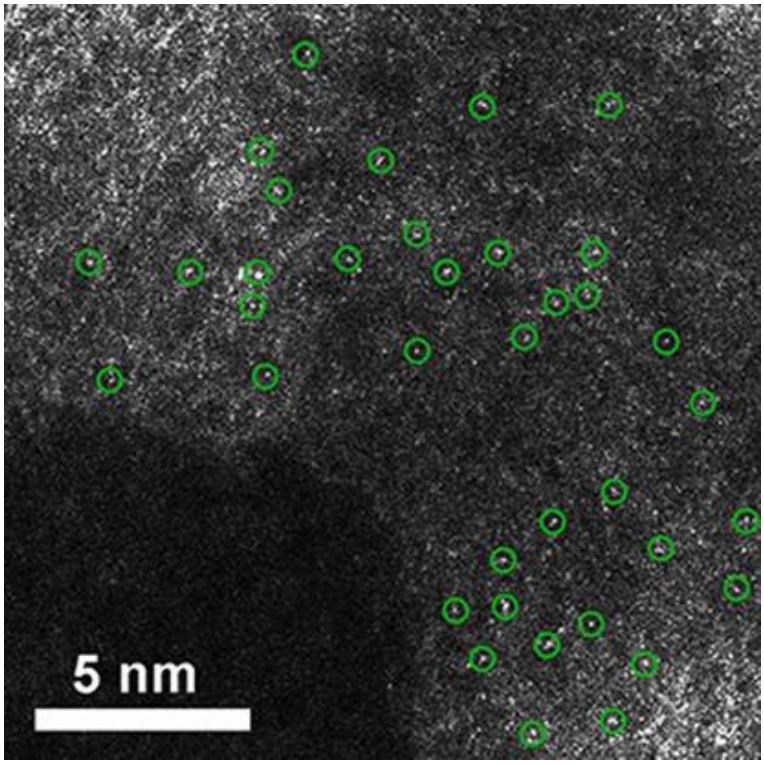

Fig. S21. AC HAADF-STEM image of Co-SAS/HOPNC after 2000 CV cycles in 0.5 M H_2SO_4 for HER. The image revealed that the Co species still kept on the N-doped carbon in the form of Co-SAs, which were identified by isolated bright dots marked with green circles.

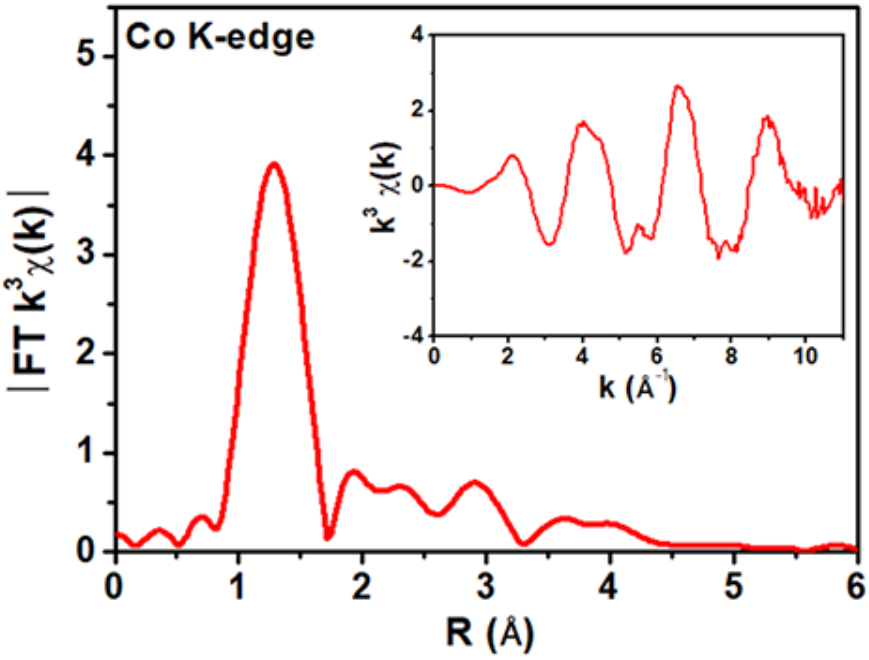

Fig. S22. Fourier transform (FT) of the Co K-edge of Co-SAS/HOPNC after 2000 CV cycles in 0.5 M H_2SO_4 for HER, inset is the corresponding EXAFS in k-space.

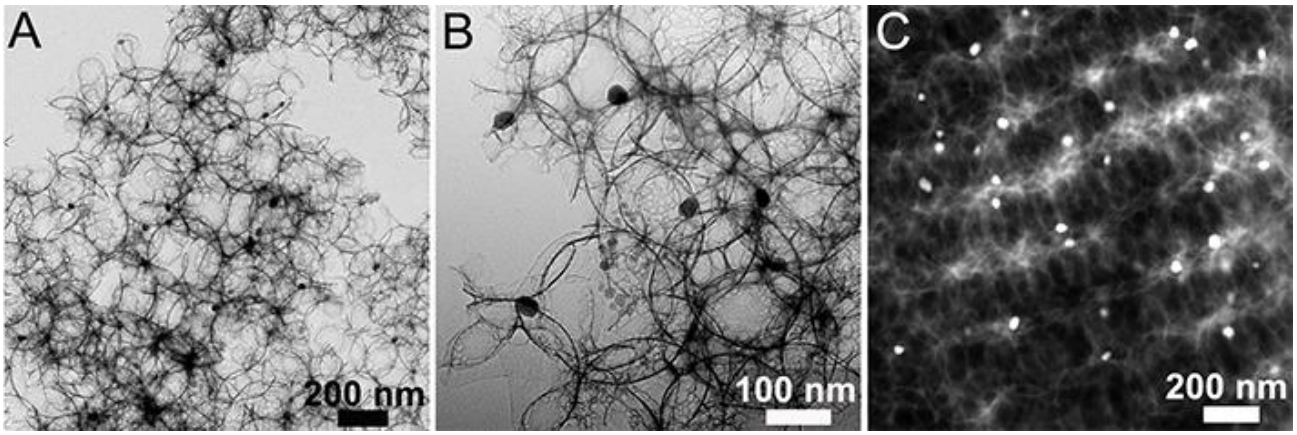

Fig. S23. (*A* and *B*) TEM, and (*C*) HAADF-STEM images of Co-NPs/HOPNC.

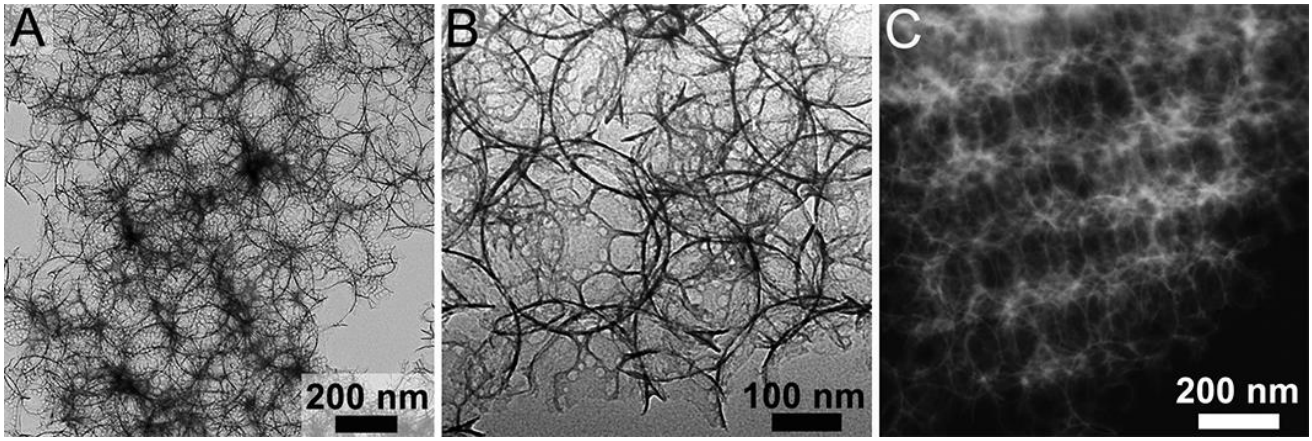

Fig. S24. (*A* and *B*) TEM, and (*C*) HAADF-STEM images of Co-NPs/HOPNC after acid leached treatment.

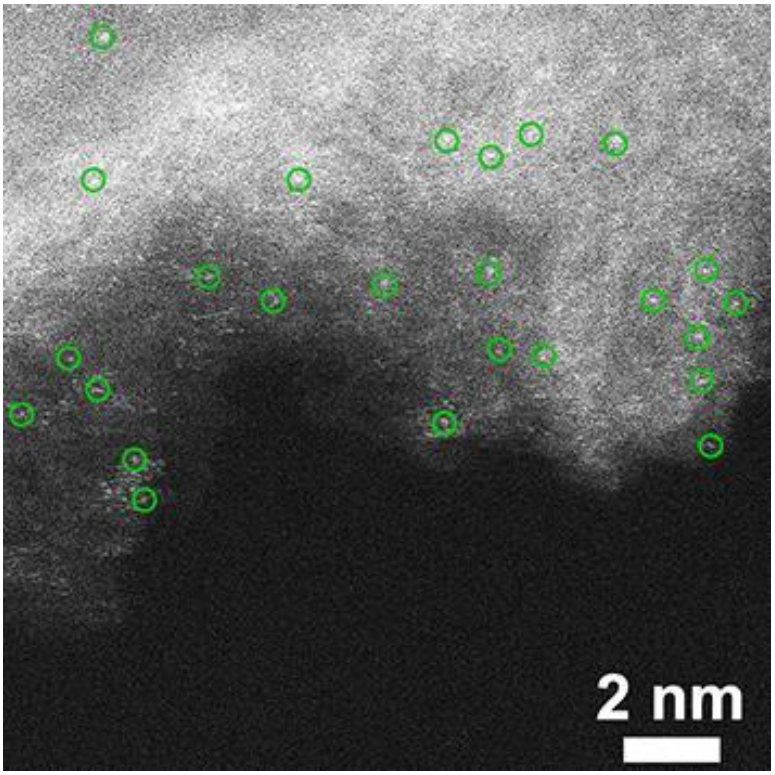

Fig. S25. AC HAADF-STEM image of Co-NPs/HOPNC after acid leaching.

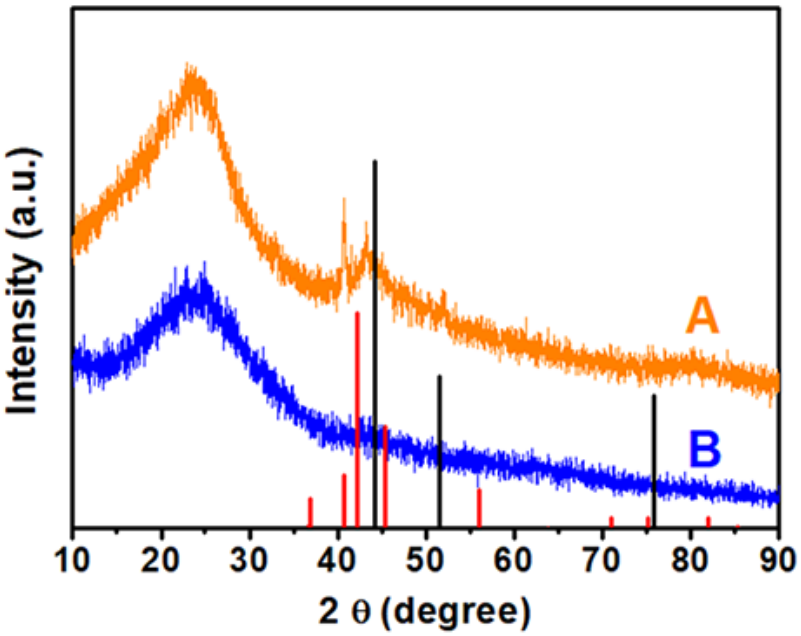

Fig. S26. XRD patterns of (*A*) Co-NPs/HOPNC and (*B*) after acid-leached Co-NPs/HOPNC with Co (JCPDS No. 15-0806, black vertical line) and Co_2C (JCPDS No. 65-8206, red vertical line) as references.

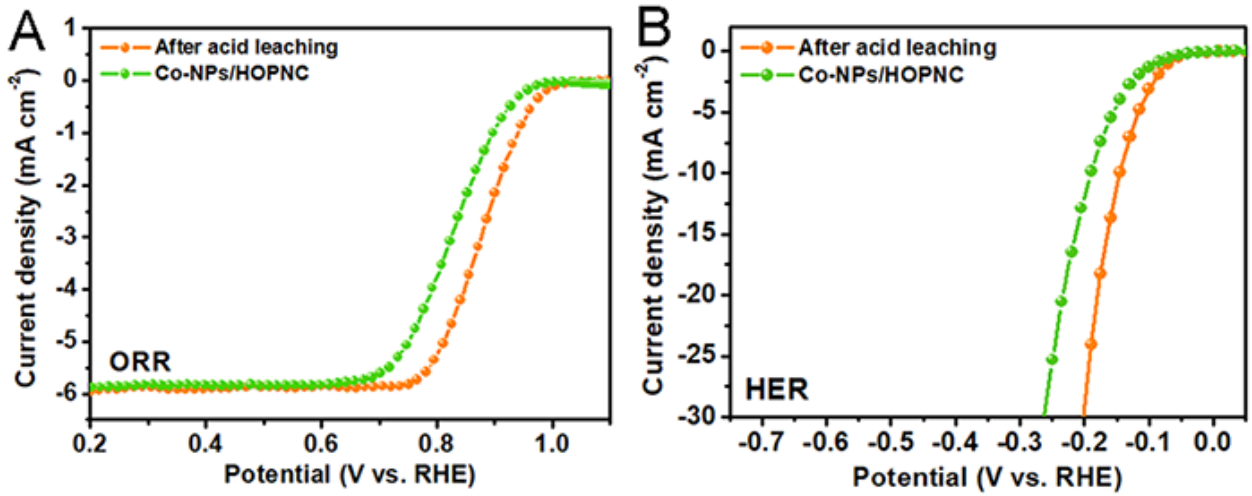

Fig. S27. (*A*) ORR and (*B*) HER polarization curves of as-prepared and acid-leached Co-NPs/HOPNC.

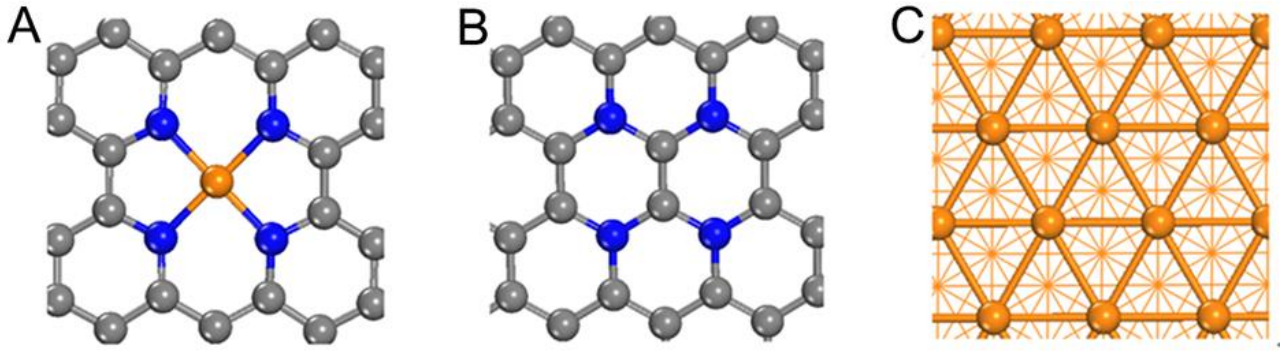

Fig. S28. Computational models of (*A*) Co-N4-C, (*B*) N4-C, and (*C*) Co-NPs (C: gray, N: blue, Co: orange)

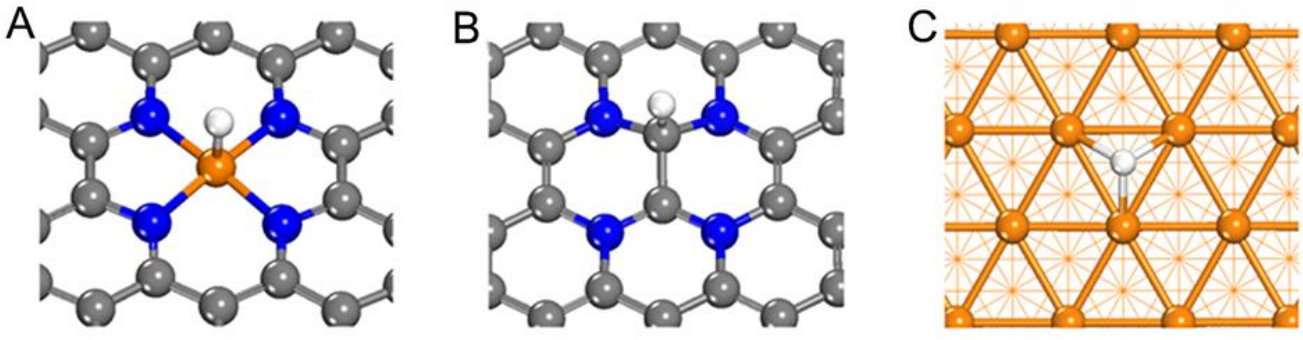

Fig. S29. Optimized structures of H adsorption on (*A*) Co-N4-C, (*B*) N4-C, and (*C*) Co-NPs (C: gray, N: blue, Co: orange, H: white).

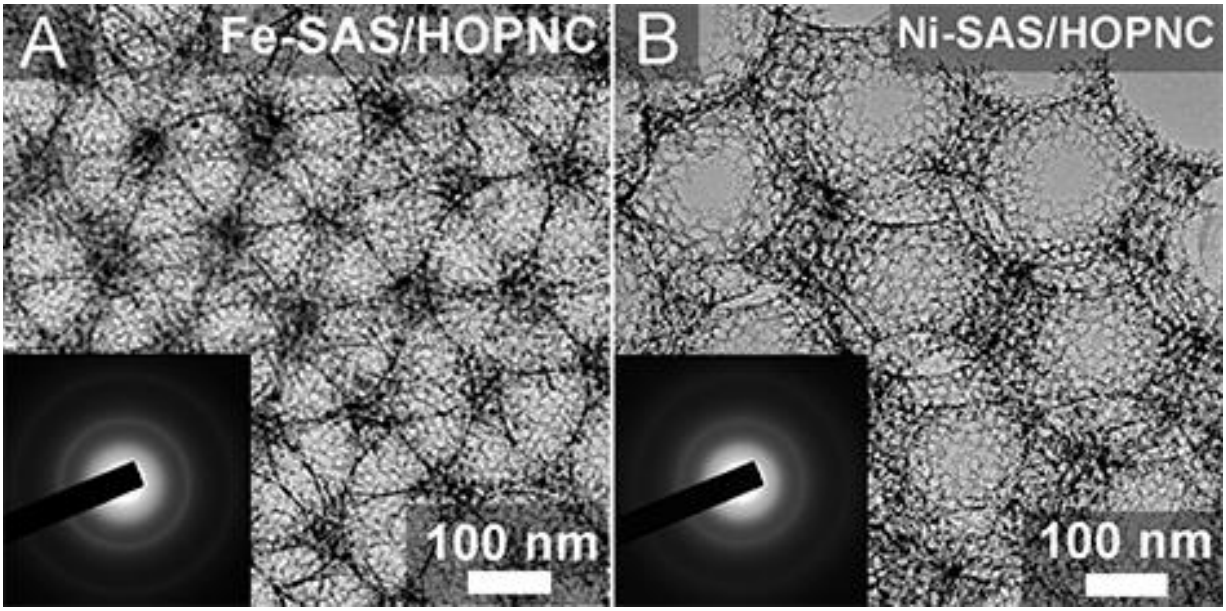

Fig. S30. TEM images of (*A*) Fe-SAS/HOPNC, and (*B*) Ni-SAS/HOPNC.

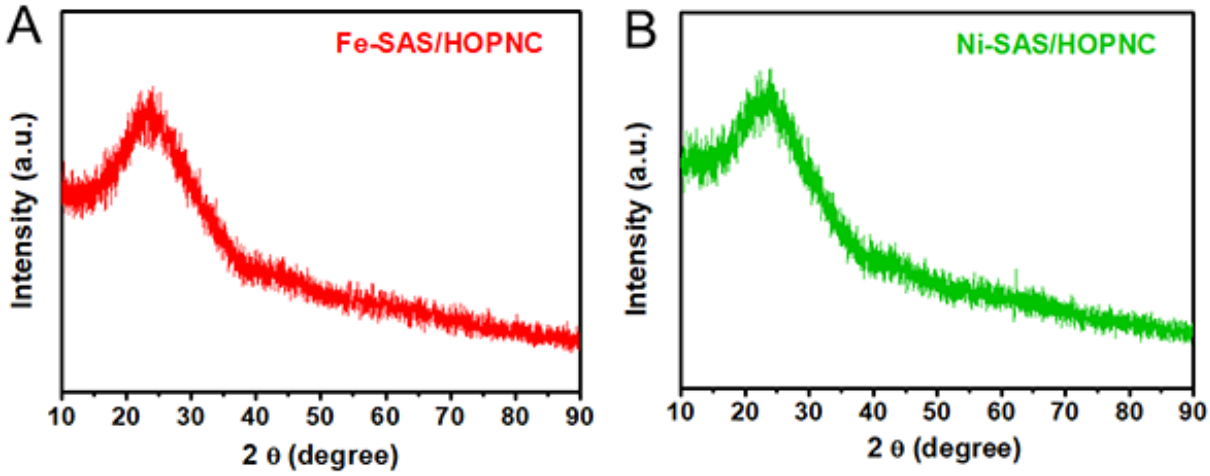

Fig. S31. XRD patterns of (*A*) Fe-SAS/HOPNC, and (*B*) Ni-SAS/HOPNC.

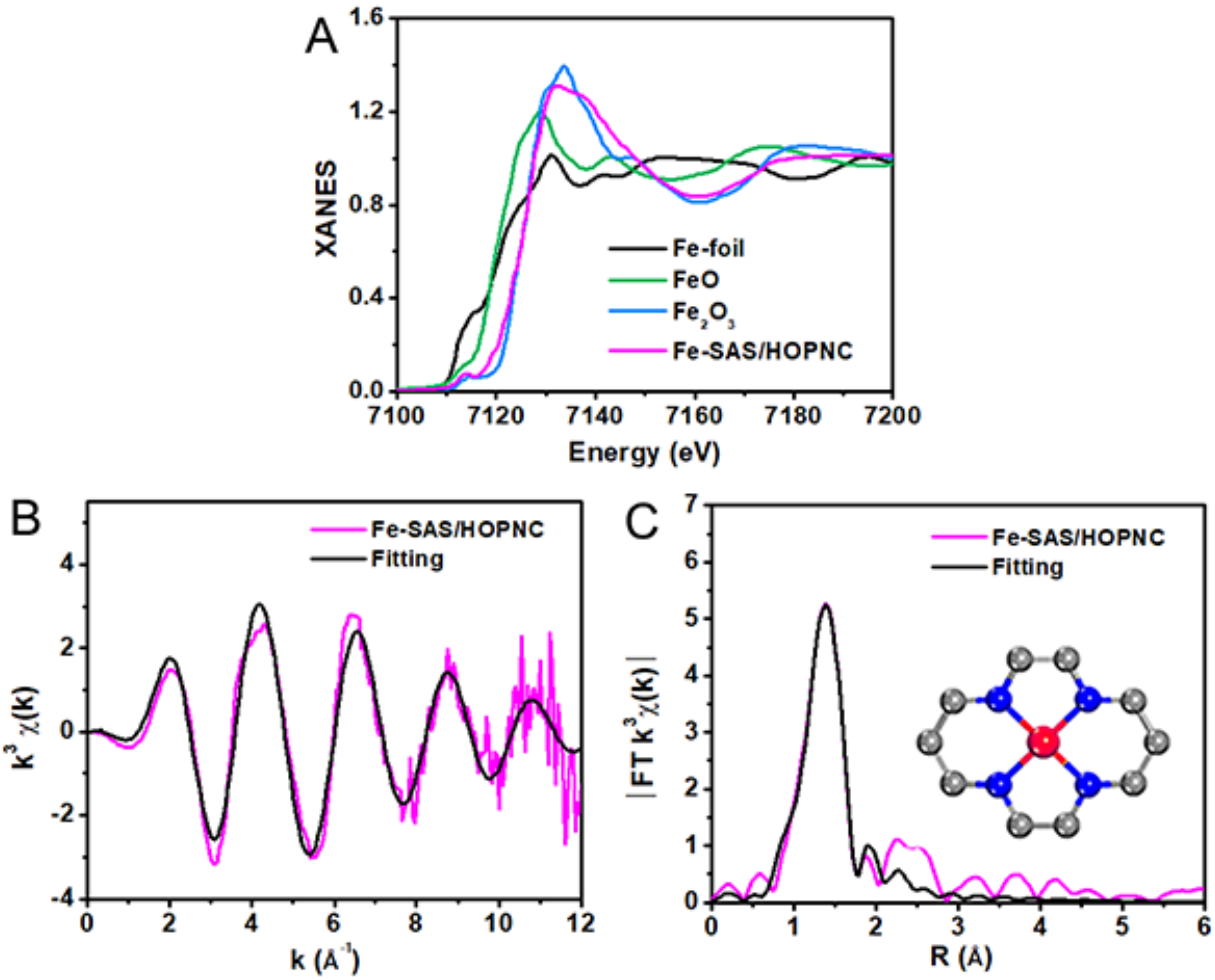

Fig. S32. (*A*) XANES spectra at the Fe K-edge of Fe-SAS/HOPNC, FeO, Fe_2O_3 sample and Fe foil. (*B*) The corresponding EXAFS fitting curves of Fe-SAS/HOPNC at *k* space. (*C*) The corresponding EXAFS fitting curves of Fe-SAS/HOPNC at *r* space, inset: schematic model of Fe-SAS/HOPNC: Fe (red), N (blue), and C (gray).

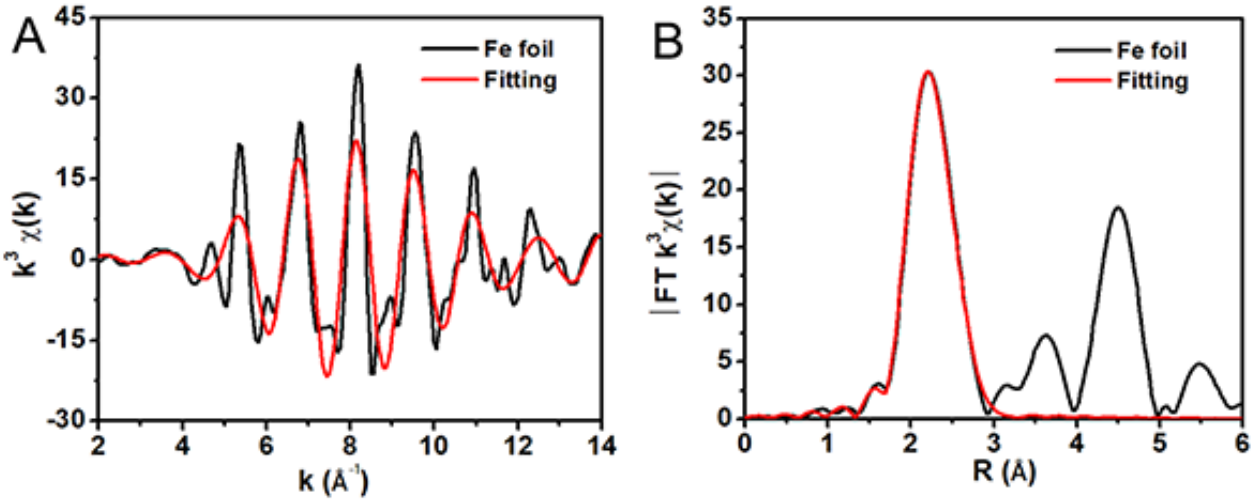

Fig. S33. The corresponding EXAFS fitting curves of Fe foil.

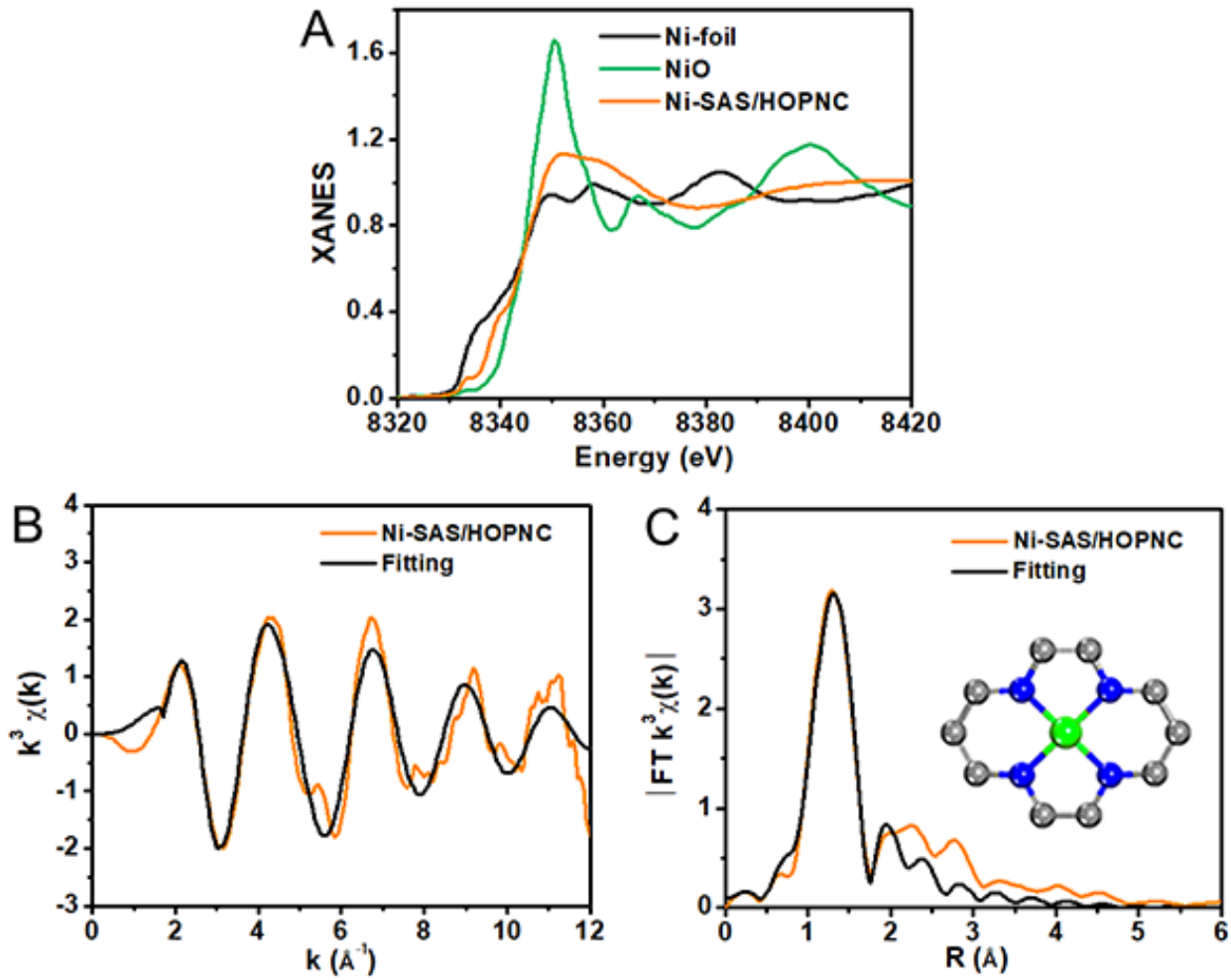

Fig. S34. (*A*) XANES spectra at the Ni K-edge of Ni-SAS/HOPNC, NiO, and Ni foil. (*B*) The corresponding EXAFS fitting curves of Ni-SAS/HOPNC at *k* space. (*C*) The corresponding EXAFS fitting curves of Ni-SAS/HOPNC at *r* space, inset: schematic model of Ni-SAS/HOPNC: Ni (green), N (blue), and C (gray).

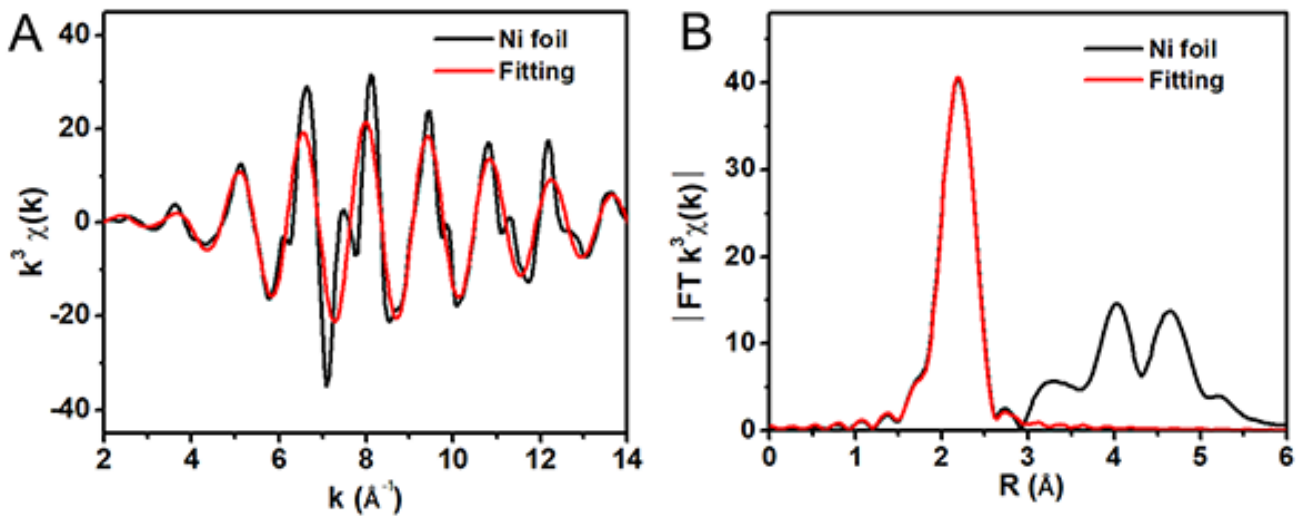

Fig. S35. The corresponding EXAFS fitting curves of Ni foil.

Table S1 ICP-OES analysis results of the as-synthesized catalysts.

Catalyst	Co (wt%)	Fe (wt%)	Ni (wt%)
Co-SAS/HOPNC	0.49		
Fe-SAS/HOPNC		0.89	
Ni-SAS/HOPNC			1.02

Table S2 Structural parameters extracted from the Co K-edge EXAFS fitting. (S_0^2=0.76).

Sample	Scattering pair	CN	R(Å)	$\sigma^2(10^{-3}Å^2)$	ΔE_0(eV)	R factor
Co-SAS/HOPNC	Co-N/C	4.1	1.96	8.9	-3.3	0.0082
Co foil	Co-Co	12*	2.50	6.5	7.7	0.0013

S_0^2 is the amplitude reduction factor; CN is the coordination number; R is interatomic distance (the bond length between central atoms and surrounding coordination atoms); σ^2 is Debye-Waller factor (a measure of thermal and static disorder in absorber-scatterer distances); ΔE_0 is edge-energy shift (the difference between the zero kinetic energy value of the sample and that of the theoretical model). R factor is used to value the goodness of the fitting.

* This value was fixed during EXAFS fitting, based on the known structure of Co foil.

Error bounds that characterize the structural parameters obtained by EXAFS spectroscopy were estimated as N ± 20%; R ± 1%; σ^2 ± 20%; ΔE_0 ± 20%.

Co-SAS/HOPNC (FT range: 2.0-11.0 $Å^{-1}$; fitting range: 1.3-2.9 Å)
Co foil (FT range: 2.0-11.0 $Å^{-1}$; fitting range: 0.7-2.1 Å)

Table S3 Comparison of the electrocatalytic ORR activity of Co-SAS/HOPNC with other representative non-noble-metal ORR electrocatalysts recently reported in the literatures.

Catalyst	Electrolyte	Loading (mg cm^{-2})	$E_{1/2}$ (V vs. RHE)	Reference
Co-SAS/HOPNC	**0.1 M KOH**	**0.6**	**0.892**	**This work**
Co-ISAS/p-CN	0.1 M KOH	N.A.	0.838	*Adv. Mater.* **2018**, 1706508.
$Co@Co_3O_4$/NC-1	0.1 M KOH	0.21	0.80	*Angew. Chem. Int. Ed.* **2016**, *55*, 4087-4091.
NPMC-1000	0.1 M KOH	0.15	0.85	*Nat. Nanotechnol.* **2015,** *10*, 444.
S,N-Fe/N/CCNT	0.1 M KOH	0.6	0.85	*Angew. Chem. Int. Ed.* **2017**, *56*, 610.
C-MOF-C2-900	0.1 M KOH	N.A.	0.82	*Adv. Mater.* **2018**, *30*, 1705431.
Fe@C-FeNC	0.1 M KOH	0.7	0.899	*J. Am. Chem. Soc.* **2016**, *138*, 3570-3578.
CNT/PC	0.1 M KOH	0.8	0.88	*J. Am. Chem. Soc.* **2016**, *138*, 15046.
CoP NCs	0.1 M KOH	0.28	0.7	*Nano Lett*. **2015**, *15*, 7616.
D-AC@2Mn-4Co	0.1 M KOH	0.08	0.792	*Adv. Mater.* **2016**, *28*, 8771.
Fe@Aza-PON	0.1 M KOH	N.A.	0.839	*J. Am. Chem. Soc.* **2018**, *140*, 1737-1742.
Co−N/CNFs	0.1 M KOH	0.1	0.82	*ACS Catal.* **2017**, *7*, 6864-6871.
Fe_3C@N-CNT	0.1 M KOH	0.25	0.85	*Energy Environ. Sci.* **2016**, *9*, 3092-3096.

Table S4 Comparison of the electrocatalytic HER activity of Co-SAS/HOPNC with other recently reported non-precious-metal HER catalysts.

Catalyst	Electrolyte	Overpotential at 10 mA cm^{-2} (mV)	Tafel slope (mV $decade^{-1}$)	Reference
Co-SAS/HOPNC	**0.5 M H_2SO_4**	**137**	**52**	**This work**
Co-NG	0.5 M H_2SO_4	147	82	*Nat. Commun.* **2015**, *6*, 8668.
$Mn_{0.05}Co_{0.95}Se_2$	0.5 M H_2SO_4	195	36	*J. Am. Chem. Soc.* **2016**, *138*, 5087.
P-1T-MoS_2	0.5 M H_2SO_4	153	43	*J. Am. Chem. Soc.* **2016**, *138*, 7965.
MoC_x nano-octahedrons	0.5 M H_2SO_4	142	53	*Nat. Commun.* **2015**, *6*, 6512.
mPF-Co-MoS_2	0.5 M H_2SO_4	156	74	*Nat. Commun.* **2017**, *8*, 14430.
Fe-Ni_3C-2%	0.5 M H_2SO_4	178	36.5	*Angew. Chem. Int. Ed.* **2017**, *56*, 1.
Ni-Co-MoS_2	0.5 M H_2SO_4	155	51	*Adv. Mater.* **2016**, *28*, 9006
Co-C-N Co mplex	0.5 M H_2SO_4	138	55	*J. Am. Chem. Soc.* **2015**, *137*, 15070.
Co-NRCNTs	0.5 M H_2SO_4	260	69	*Angew. Chem. Int. Ed.* **2014**, *53*, 4372.
Mo_2C@NC	0.5 M H_2SO_4	124	60	*Angew. Chem. Int. Ed.* **2015**, *54*, 10752.
M-MoS_2	0.5 M H_2SO_4	175	41	*Nat. Commun.* **2016**, *7*, 10672.
Co_2P-C	0.5 M H_2SO_4	96	68	*J. Am. Chem. Soc.* **2017**, *139*, 11248.

Table S5 TOF values of the Co-SAS/HOPNC for HER and other electrocatalysts.

Catalyst	**Electrolyte**	TOF (s^{-1})	**Reference**
Co-SAS/HOPNC	0.5 M H_2SO_4	0.41 (100 mV) 3.80 (200 mV)	This work
Co-NG	0.5 M H_2SO_4	0.101 (100 mV)	*Nat. Commun.* **2015**, *6*, 8668.
CoP/Ti	0.5 M H_2SO_4	0.046 (100 mV)	*Angew. Chem. Int. Ed.* **2014**, *53*, 5427.
Ni@NC	0.5 M H_2SO_4	0.34 (350 mV)	*Adv. Energy Mater.* **2015**, *5*, 1401660.
$[Mo_3S_{13}]^{2-}$ ⁞ GP	0.5 M H_2SO_4	0.59 (200 mV)	*Nat. Chem.* **2014**. *6*. 248.
UHV MoS_2 ⁞ Au(111)	0.5 M H_2SO_4	0.90 (100 mV)	*Science* **2007**, *317*, 100.
P-1T MoS_2	0.5 M H_2SO_4	0.50 (153 mV)	*J. Am. Chem. Soc.* **2016**, *138*, 7965.
$Fe_{0.9}Co_{0.1}S_2$/CNT	0.5 M H_2SO_4	0.31 (170 mV)	*J. Am. Chem. Soc.* **2015**, *137*, 1587.
Ni_2P	0.5 M H_2SO_4	0.05 (100 mV) 0.36 (200 mV)	*J. Am. Chem. Soc.* **2013**, *135*, 9267.

Table S6 Adsorption energies (eV) of different intermediates during ORR on Co-N_4 and Co (111), which were calculated using clean active sites, gaseous H_2O, and H_2 as reference.

	Co-N_4	**Co (111)**
O	2.46	-0.11
OH	0.90	-0.05
OOH	3.83	2.87

Table S7 Zero point energies (ZPE) and entropy contribution (TS) for different intermediates on Co-N_4 site (T=298K).

	HO*	O*	HOO*
ZPE (eV)	0.34	0.06	0.44
TS (eV)	0.13	0.08	0.20

Table S8 Zero point energies (ZPE) and entropy contribution (TS) for different intermediates on Co (111) (T=298K).

	HO*	O*	HOO*
ZPE (eV)	0.35	0.07	0.37
T*S (eV)	0.07	0.04	0.23

Table S9 Structural parameters extracted from the Fe K-edge EXAFS fitting. (S_0^2=0.76).

Sample	Scattering pair	CN	R(Å)	$\sigma^2(10^{-3}Å^2)$	ΔE_0(eV)	R factor
Fe-SAS/HOPNC	Fe-N/C	4.1	1.95	6.7	-1.5	0.005
Fe foil	$Fe-Fe_1$	8*	2.45	4.2	2.0	0.003
	$Fe-Fe_2$	6*	2.86	5.4		

S_0^2 is the amplitude reduction factor; CN is the coordination number; R is interatomic distance (the bond length between central atoms and surrounding coordination atoms); σ^2 is Debye-Waller factor (a measure of thermal and static disorder in absorber-scatterer distances); ΔE_0 is edge-energy shift (the difference between the zero kinetic energy value of the sample and that of the theoretical model). R factor is used to value the goodness of the fitting.

* This value was fixed during EXAFS fitting, based on the known structure of Fe foil.

Error bounds that characterize the structural parameters obtained by EXAFS spectroscopy were estimated as N ± 20%; R ± 1%; σ^2 ± 20%; ΔE_0 ±20%.

Fe-SAS/HOPNC (FT range: 2.0-11.5 $Å^{-1}$; fitting range: 0.8-2.0 Å)
Fe foil (FT range: 2.0-12.4$Å^{-1}$; fitting range: 1.4-3.0 Å)

Table S10 Structural parameters extracted from the Ni K-edge EXAFS fitting. (S_0^2=0.76).

Sample	Scattering pair	CN	R(Å)	$\sigma^2(10^{-3}Å^2)$	ΔE_0(eV)	R factor
Ni-SAS/HOPNC	Ni-N/C	3.9	1.93	5.5	-1.0	0.003
Ni foil	Ni-Ni	12*	2.47	4.8	2.5	0.002

S_0^2 is the amplitude reduction factor; CN is the coordination number; R is interatomic distance (the bond length between central atoms and surrounding coordination atoms); σ^2 is Debye-Waller factor (a measure of thermal and static disorder in absorber-scatterer distances); ΔE_0 is edge-energy shift (the difference between the zero kinetic energy value of the sample and that of the theoretical model). R factor is used to value the goodness of the fitting.

* This value was fixed during EXAFS fitting, based on the known structure of Ni foil.

Error bounds that characterize the structural parameters obtained by EXAFS spectroscopy were estimated as N ± 20%; R ± 1%; σ^2 ± 20%; ΔE_0 ± 20%.

Ni-SAS/HOPNC (FT range: 2.0-10.5 $Å^{-1}$; fitting range: 0.5-2.0 Å)
Ni foil (FT range: 2.0-14.0 $Å^{-1}$; fitting range: 1.4-3.0 Å)